Single-component immunomodulatory hyaluronic acid hydrogel patch for accelerated chronic wound healing application

Shima Tavakoli, Mahshid Shokri, Yulai Xia, Mohsen Ahmadi Tafti, Oommen P. Oommen, Mahshid Kharaziha, Oommen P. Varghese

PII: S0168-3659(26)00752-2

DOI: https://doi.org/10.1016/j.jconrel.2026.115348

Reference: COREL 115348

To appear in: *Journal of Controlled Release*

Received date: 16 March 2026

Revised date: 23 August 2026

Accepted date: 9 September 2026

Please cite this article as: S. Tavakoli, M. Shokri, Y. Xia, et al., Single-component immunomodulatory hyaluronic acid hydrogel patch for accelerated chronic wound healing application, *Journal of Controlled Release* (2026), https://doi.org/10.1016/j.jconrel.2026.115348

Single-Component Immunomodulatory Hyaluronic Acid Hydrogel Patch for Accelerated Chronic Wound Healing Application

Shima Tavakoli[1], Mahshid Shokri[2,3], Yulai Xia[4], Mohsen Ahmadi Tafti[5], Oommen P. Oommen[6], Mahshid Kharaziha[2], Oommen P. Varghese[1*]

[1]Translational Chemical Biology Group, Science for Life Laboratory, Division of Macromolecular Chemistry, Department of Chemistry-Ångstrom Laboratory, Uppsala University, Uppsala SE75121, Sweden

[2]Department of Materials Engineering, Isfahan University of Technology, Isfahan 84156-83111

[3]Research Center for Advanced Technologies in Cardiovascular Medicine, Tehran Heart Center, Tehran, Iran

[4]Department of Chemistry, Universität Konstanz, Konstanz, Germany

[5]Division of Colorectal Surgery, Department of Surgery, Tehran University of Medical Sciences, Tehran, Iran

[6]School of Pharmacy and Pharmaceutical Sciences, Cardiff University, Cardiff, CF10 3NB UK

Abstract

Chronic wounds often suffer from persistent inflammation, which hinders tissue regeneration. In this study, we present a multifunctional hyaluronic acid (HA)–based hydrogel patch with controlled reactive oxygen species (ROS) scavenging and immunomodulatory properties to accelerate chronic wound healing. A novel single-component strategy was developed in which HA was simultaneously modified with carbodihydrazide groups and gallic acid (GA) derivatives. We demonstrate, for the first time, that hydrogel formation can occur solely from carbodihydrazide-modified HA, without the need for an aldehyde-functionalized counterpart. Incorporation of GA not only consolidated hydrogel formation but also enabled material fabrication with tunable shapes and high fluid-absorbance capacity, as well as intrinsic antioxidant and immunomodulatory activities. This design offers significant clinical advantages by providing a user-friendly, ready-to-apply wound dressing that eliminates the need for precursor mixing, ensuring reproducibility and ease of use. In vitro studies further revealed that treatment of pro-inflammatory macrophages (M1) with the hydrogel formulations promoted a phenotypic shift toward anti-inflammatory M2 macrophages. When applied to chronic wounds in vivo, the multifunctional HA hydrogel patch effectively scavenged ROS, suppressed inflammation, and established a favorable microenvironment for tissue repair and regeneration.

Keywords: hydrogel, hyaluronic acid, chronic wound, immunomodulation, antioxidant

1. Introduction

Chronic wounds, often associated with persistent hyperglycemia, represent a major clinical challenge that significantly affects patient prognosis and quality of life [1]. Wound healing is inherently a complex and highly regulated process that relies on the coordinated activation, recruitment, and function of various cell types, including keratinocytes, endothelial cells, fibroblasts, and immune cells, along with the interplay of growth factors, cytokines, and chemokines [2]. Under normal conditions, the skin demonstrates a remarkable regenerative capacity, undergoing a dynamic, multistep process that involves hemostasis, inflammation, proliferation, and remodeling phases [3]. However, proper regulation of the immune microenvironment is essential for successful healing. When this regulation is disrupted, wound healing becomes impaired, resulting in chronic wounds characterized by unresolved inflammation [4]. Such delays in healing often stimulate excessive secretion of pro-inflammatory cytokines and cause a marked increase in mitochondrial reactive oxygen species (ROS). In vivo studies have demonstrated the presence of heterogeneous macrophage subpopulations displaying both M1 and M2 phenotypes in the wound healing process [2]. Following injury, M1 macrophages rapidly infiltrate the wound, with their numbers peaking between days 7 and 14 of the healing process. Their activation is driven by IFN-γ and microbial stimuli, leading to the release of cytokines including TNF-α, IL-6, IL-12, and CCL2 [5]. However, if M1 persistence and ROS overproduction are not adequately controlled, the healing process becomes stalled in a state of chronic inflammation. This impairs the critical transition from the regenerative to the resolving phase, often resulting in excessive scarring or abnormal granulation tissue formation, such as keloids [6]. Therefore, precise regulation of both ROS levels and macrophage phenotypes is essential to ensure successful wound healing. Recent therapeutic strategies have thus focused on modulating the wound microenvironment by attenuating oxidative stress and promoting a balanced macrophage polarization toward the pro-regenerative M2 phenotype.

Hydrogels, with their hydrophilic three-dimensional (3D) network structures, represent an ideal class of wound dressings, as they can efficiently absorb wound exudates, ensure breathability, and maintain a moist environment that supports healing [4]. Among the various materials used for hydrogel construction, hyaluronic acid (HA), a highly hydrated glycosaminoglycan abundantly present in the extracellular matrix (ECM), has received significant attention [7]. HA interacts with multiple cellular receptors to trigger key biological responses and has been widely associated with enhanced cell migration, proliferation, angiogenesis, and tissue regeneration [8]. These unique properties make HA an attractive candidate for engineering hydrogels tailored for effective wound repair. However, HA-based materials inherently suffer from weak mechanical strength and limited long-term stability, which restricts their direct application as wound dressings [9]. To address these shortcomings, various crosslinking strategies have been developed,

among which the formation of hydrazone bonds has been widely explored over the past decade [7]. Hydrazone crosslinking offers several advantages, including its ability to form under near physiological conditions, especially in carboxylated polymers and in the presence of salts [10]. Moreover, small molecules bearing hydrazide and hydrazone functionalities have been reported to exhibit intrinsic antioxidant and antibacterial activity [11,12]. In addition, carbazate-modified polymers have been shown to scavenge reactive aldehyde byproducts from the surrounding environment [13]. Hydrazone formation relies on dynamic covalent interactions between aldehyde- and hydrazide-functionalized HA chains, requiring prior chemical modification of HA with these two distinct groups. Despite its effectiveness, this approach poses practical challenges, as the reaction proceeds extremely rapidly, often within 30 seconds, leaving little time for thorough mixing of the precursors and resulting in heterogeneous hydrogel formation [10,14,15]. Limited hydrolytic stability is another challenge to designing stable products. We have previously demonstrated that carbodihydrazide-derived hydrazone linkages lead to more efficient crosslinking due to enhanced delocalization of charges, resulting in hydrolytically stable materials [14,16]. Clinically, however, the development of hydrogel systems derived from a single precursor is more desirable as it eliminates the need for dual-component mixing.

In addition to providing a stable hydrogel network for wound healing applications, effective treatment of chronic wounds also requires materials to have intrinsic anti-inflammatory properties. Traditionally, this has been addressed by incorporating small-molecule drugs into hydrogel matrices to modulate immune activity [17,18]. While such strategies have demonstrated some therapeutic benefit, limitations remain regarding controlled release kinetics and sustained long-term effects. Recently, diabetic wound treatment has been explored using a sulfonated HA system modified with carbodihydrazide and aldehyde groups, in which hydrazone crosslinking occurs upon physically incorporating TGF-β1 and berberine as drug molecules [19]. However, this approach still depends on loaded therapeutic drugs in the hydrogel network. An alternative and more effective approach would be to endow the hydrogel backbone itself with these bioactive functions. Gallic acid (GA), a naturally occurring polyphenolic compound, is widely employed for conjugation with natural polymers owing to its diverse biological activities, including antioxidant, antibacterial, and anti-inflammatory effects [20,21]. The phenolic hydroxyl groups of GA contribute to its strong free radical scavenging capacity, facilitated by quinone formation and stabilization of free radicals by delocalization of electrons within the aromatic ring, thereby conferring potent antioxidant properties [22]. Conjugating GA to HA not only enhances the stability and mechanical properties of hydrazone-crosslinked hydrogels but also imparts ROS-quenching activity and promotes immunosuppressive, M2-like macrophage polarization, as we have shown recently [23]. Together, these features suggest strong potential of such biomaterials for treating chronic wounds and promoting tissue healing.

In this study, we propose a novel strategy for developing a single-component hydrogel-based wound dressing to treat hard-to-heal wounds. Specifically, HA was simultaneously modified with carbodihydrazide groups and GA derivatives. For the first time, we demonstrate that hydrogel formation can be achieved solely from carbodihydrazide-modified HA, without the need for an additional aldehyde-functionalized counterpart. Moreover, the incorporation of the GA derivative onto the HA backbone imparts inherent antioxidant and anti-inflammatory properties to the network. This easy-to-apply multifunctional hydrogel patch is expected to suppress inflammation and thereby promote a favorable microenvironment for effective tissue regeneration (Figure 1a).

2. Results and discussion

2.1. Synthesis and characterization of modified HA hydrogels

HA is a naturally occurring glycosaminoglycan that is abundantly distributed throughout the body, with particularly high concentrations in the skin, where it plays a crucial role in tissue hydration, remodeling, and wound healing [24]. To develop a bioactive hydrogel matrix tailored for chronic wound healing, we selected HA as the base biopolymer due to its inherent biocompatibility and wound healing potential. To develop an HA-based biomaterial that allows self-crosslinking and imparts immunomodulatory properties, we chemically modified the HA carboxylate with carbodihydrazide and GA derivative moieties. Carbodihydrazide-modified HA (HA-C polymer) was synthesized using carbodiimide coupling chemistry, as we have reported previously [25]. The degree of hydrazide modification was quantified using the trinitrobenzene sulfonic acid (TNBS) assay, which measures free primary amines. The modification degree was calculated to be approximately 20%. Since HA has free aldehyde units at the reducing end, we envisioned that excess hydrazide groups in the polymer backbone could yield a hydrogel network via hydrazone chemistry without the addition of other modified polymers (Figure 1b).

To confirm that hydrogel formation was driven primarily by the reaction between hydrazide groups and terminal aldehyde groups on the HA backbone, HA-C hydrogels were formed and subjected to a range of different conditions to evaluate hydrogel stability (Supporting Information, Table S1). The HA-C hydrogel remained stable in PBS at pH 7.4, indicating compatibility with physiological conditions. When incubated in PBS supplemented with 1 M NaCl, the hydrogel retained its structure, suggesting that electrostatic interactions were not the main reason for gel formation. Similarly, the gel remained stable in PBS containing 1 M urea, ruling out hydrogen bonding as the dominant factor in network stabilization. Interestingly, the hydrogel dissolved within a few hours under acidic conditions (pH 3), while it exhibited greater stability in a basic environment (pH 11). These observations support the involvement of pH-sensitive hydrazone bonds, which are known to be more stable at basic pH and susceptible to hydrolysis in acidic environments [26].

Together, these findings confirm that the hydrogel is primarily formed through hydrazone linkages between hydrazide groups and terminal aldehydes on the HA chains.

To demonstrate the intrinsic gel-forming capability of HA-C without the need for additional crosslinkers and also the role of solid content, hydrogels were prepared at varying solid contents of 2%, 4%, 8%, and 12% (w/v). Rheological characterization using amplitude sweep analysis in Figure 2a revealed that at a 2% solid content, the hydrogel exhibited weak mechanical properties, with a storage modulus (G′) of less than 100 Pa, indicating a loosely cross-linked network. However, as the solid content increased, the stiffness of the hydrogels improved significantly as the polymer chains were closer to each other. At 12% solid content, the hydrogel exhibited a storage modulus of 7346±1233 Pa, reflecting a more robust and well-structured network (Figure 2a). This concentration-dependent enhancement in mechanical strength supports the role of hydrazide-mediated self-crosslinking in HA-C hydrogels and highlights the tunability of their mechanical properties through polymer concentration.

Further evidence supporting this mechanism was obtained through control experiments. A 12% hydrogel formed from unmodified HA showed poor mechanical integrity, with a G′ below 100 Pa (Figure 2b), indicating that HA alone is insufficient to form a stable network. To validate this further, we first reduced the terminal aldehyde groups with sodium borohydride, followed by chemical modification of the carboxylate units with carbodihydrazide modification (RHA-C polymer). When this modified polymer was used to prepare a hydrogel at 12% (w/v) solid content, the resulting RHA-C hydrogel exhibited a modulus approximately four-fold lower than that of the corresponding HA-C hydrogel containing the native reducing-end aldehyde groups (Figure 2b). This substantial reduction in G′ highlights the important contribution of terminal aldehyde groups to hydrazone-mediated crosslinking and network formation. Nevertheless, RHA-C was still capable of forming a self-supporting hydrogel. Several factors may explain this observation. First, complete reduction of all terminal aldehyde groups is challenging due to their low abundance and limited accessibility along the HA chains. As a result, a fraction of residual aldehyde functionalities may remain available to participate in hydrazone bond formation. Second, presence of excess hydrazide residues could contribute to form hydrogen-bonds with available carboxylate residues. Together, these effects may contribute to the formation of a weaker, yet still continuous, hydrogel network following the reduction treatment. Direct quantification of this residual aldehyde pool is not experimentally straightforward, as the reducing end of HA exists in a dynamic equilibrium between the closed pyranose (hemiacetal) form, which dominates in aqueous solution, and the reactive open-chain aldehyde tautomer, which is present only transiently and in low relative abundance. Because each HA chain carries only a single reducing end regardless of its molecular weight, the resulting terminal-group molar fraction is intrinsically very low, placing it below the reliable quantification range of derivatization-based assays such as TNBS or

the detection limit of FTIR and solution-state NMR. We have therefore relied on the converging chemical (Table S1) and mechanical (Figure 2b) evidence described above to support hydrazone-bond formation as the dominant gelation mechanism.

Although this was interesting, we decided to incorporate GA moieties on the same HA backbone to provide additional stability and functionality. GA is conventionally grafted to HA either through esterification of aliphatic hydroxyls or via carbodiimide-mediated conjugation of amine-functionalized GA to the carboxyl groups of HA. However, both approaches typically suffer from low coupling efficiency [27,28]. To overcome this, we synthesized a GA derivative having hydrazide functionality (-NH-NH_2), enabling more efficient carbodiimide coupling due to the lower pKa of hydrazides as compared to primary amines, an approach we recently reported [29]. Introduction of both hydrazide and GA moieties onto the HA backbone produced a dual-functionalized derivative (HA-CG polymer). This strategy enables hydrogel formation from a single polymer species (HA-CG), simplifying formulation and potentially improving uniformity and reproducibility. The degree of GA derivatives modification was determined by ^{1}H NMR spectroscopy. By integrating the aromatic peaks of GA relative to the methyl protons of N-acetyl units of HA, the degree of substitution was estimated to be 10% (Supporting Information, Figure S1).

Interestingly, as shown in Figure 2b, the introduction of GA derivative groups alongside hydrazide groups on the HA backbone further enhanced the mechanical properties of the hydrogel. The resulting HA-CG hydrogel exhibited a significantly higher storage modulus (9026 ± 1082 Pa) compared to HA-C alone, indicating a stiffer and more robust network. This enhancement is attributed to the presence of GA derivatives, which are known to undergo oxidative coupling and potentially form additional covalent or non-covalent interactions within the hydrogel matrix [20,28]. These interactions likely contribute to obtaining a denser and more crosslinked network structure, reinforcing the gel and improving its mechanical integrity. The dual-functionalization strategy offers a simple yet effective means of tuning hydrogel properties. Importantly, the ability to generate mechanically strong hydrogels from a single HA-based polymer without the need for additional crosslinkers provides an efficient approach for designing bioactive scaffolds.

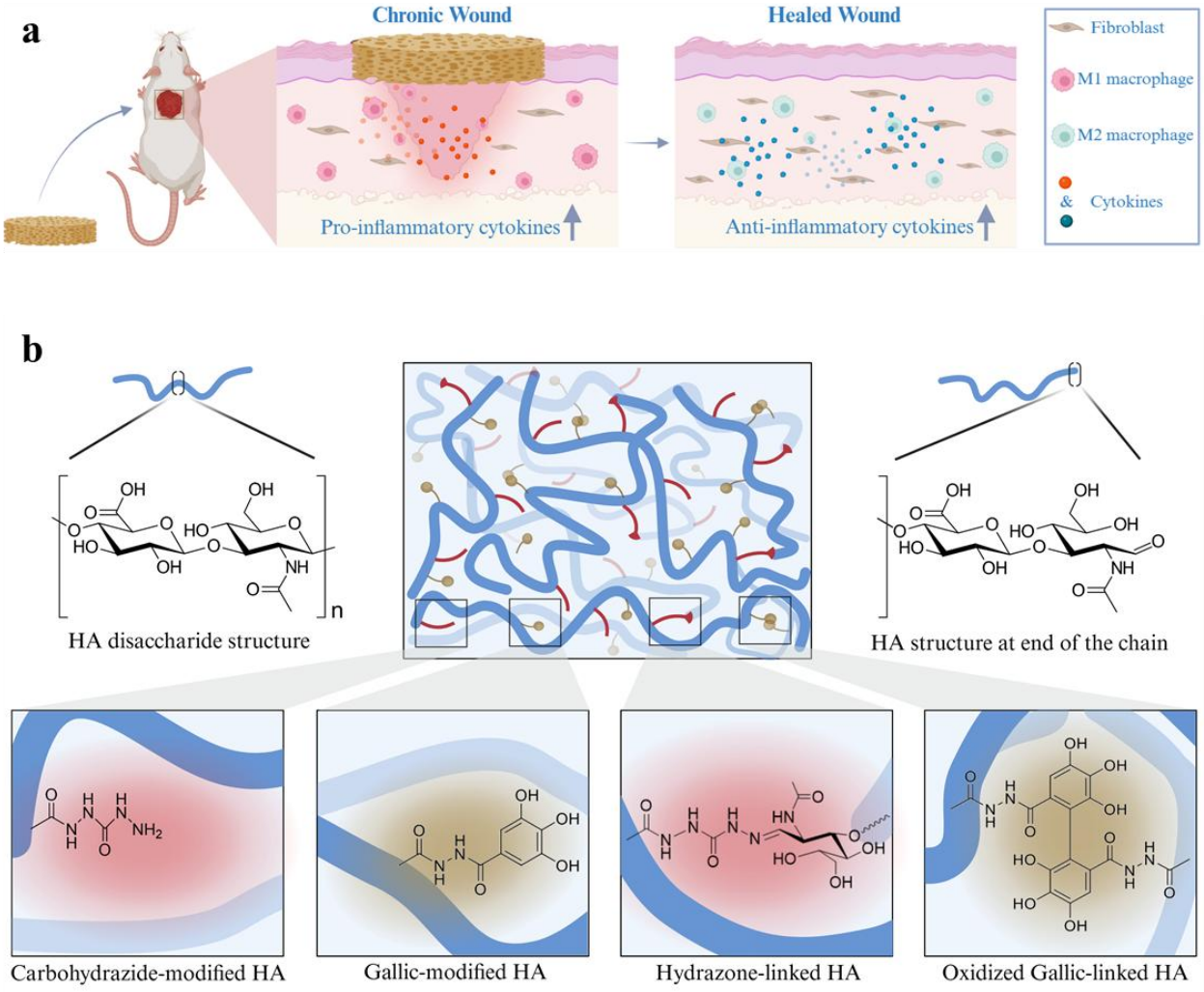

Figure 1. Schematic representation of the developed wound dressing and hyaluronic acid (HA) modification. a) Illustration of the wound dressing patch applied in an animal model, showing its ability to regulate healing by controlling the wound microenvironment. b) Structural representation of the disaccharide unit of HA, highlighting a random site along the polymer chain as well as the terminal end. Schematic depiction of HA modification via carbodiimide coupling chemistry to introduce hydrazide and gallic acid derivative groups, followed by crosslinking through hydrazone bond formation and oxidation of gallic groups.

To evaluate the long-term stability of the hydrogels under physiological conditions, samples were incubated in PBS (pH 7.4) at 37 °C. As shown in Figure 2c, the hydrogel formed from reduced HA ($NaBH_3$-treated) modified with hydrazide groups with 12% solid content (RHA-C) degraded rapidly, fully dissolving within 2 days. This was expected due to the absence of terminal aldehyde groups, which are essential for hydrazone crosslinking. Stability was also found to be highly dependent on the solid content of the hydrogel. HA-C hydrogels with lower polymer concentrations exhibited reduced stability; the 4% (HA-C4) and 8% (HA-

C8) gels degraded completely after approximately 2 and 16 days, respectively. In contrast, when the solid content was increased to 12% (HA-C12), the hydrogel remained stable for over 128 days, demonstrating that higher polymer content leads to a denser and more durable network. Similarly, HA-CG hydrogels prepared at 12% solid content (HA-CG12) also remained stable beyond 128 days. However, overall, HA-CG12 exhibited a lower swelling ratio compared to HA-C12 (>700% for HA-CG12 and >2000% for HA-C12 after 28 days of experiment), which may be attributed to additional crosslinking interactions introduced by the GA derivative groups. Based on their superior mechanical strength and long-term stability, HA-C12 and HA-CG12 hydrogels were selected as the representative formulations for further experiments.

Next, the swelling and stability behavior of HA-C and HA-CG hydrogels (both at 12% solid content) was evaluated in cell culture medium. As shown in Figure 2d, both formulations exhibited high swelling capacity while maintaining structural integrity for over 128 days, with the ratio of 623±198% for HA-C and 512±83% for HA-CG hydrogels. Notably, the HA-C hydrogel showed a sharp increase in swelling after day 8, suggesting a relaxation or loosening of the network over time. In contrast, the HA-CG hydrogel exhibited a more gradual and controlled swelling profile, consistent with the presence of a more stabilized and tightly crosslinked network.

To assess enzymatic degradation, both hydrogels were incubated in hyaluronidase solution, which specifically cleaves the HA backbone [30,31]. As shown in Figure 2e, both formulations were biodegradable in the presence of the hyaluronidase enzyme. However, HA-C hydrogels fully degraded after 5 days, whereas HA-CG hydrogels remained intact for up to 9 days before complete dissolution. This extended degradation time further supports the hypothesis that HA-CG possesses a denser and more robust crosslinked structure compared to HA-C, likely due to the additional stabilizing interactions provided by the GA derivatives moieties. The HA-CG hydrogel exhibited high stability in PBS, whereas degradation was observed in the presence of hyaluronidase. This behavior suggests that the release of GA-containing moieties is primarily governed by enzymatic degradation of the HA backbone rather than by the diffusion of free GA derivatives. Since the GA groups are covalently grafted onto the HA chains, they are not expected to be released as free molecules under physiological conditions. Instead, upon enzymatic cleavage of the HA network by hyaluronidase secreted by cells or present in vivo, smaller HA fragments containing covalently attached hydrazide and GA moieties may be generated and interact with surrounding cells and tissues. Therefore, the biological activity of the hydrogel is closely linked to the degradation behavior of the HA matrix.

To explore the potential of these hydrogel formulations as wound dressings, the as-prepared gels were subjected to snap-freezing followed by lyophilization. The resulting dry scaffolds can be used as wound dressing materials with the ability to rehydrate upon application (Figure 2f). Figures 2g and 2h show the

lyophilized samples at day 0 and their corresponding swelling profiles in cell culture medium. Both HA-C and HA-CG scaffolds demonstrated a high capacity to absorb the surrounding medium and retain it within the gel matrix, when compared with their initial dried weight (Supporting Information, Figure S2). This absorbent behavior is particularly advantageous for chronic wound applications, where the management of excess wound exudate is a major clinical challenge. The ability of these scaffolds to uptake and hold fluids suggests their suitability as bioactive, hydrating wound dressings that can maintain a moist environment, an important factor for promoting tissue regeneration and wound healing.

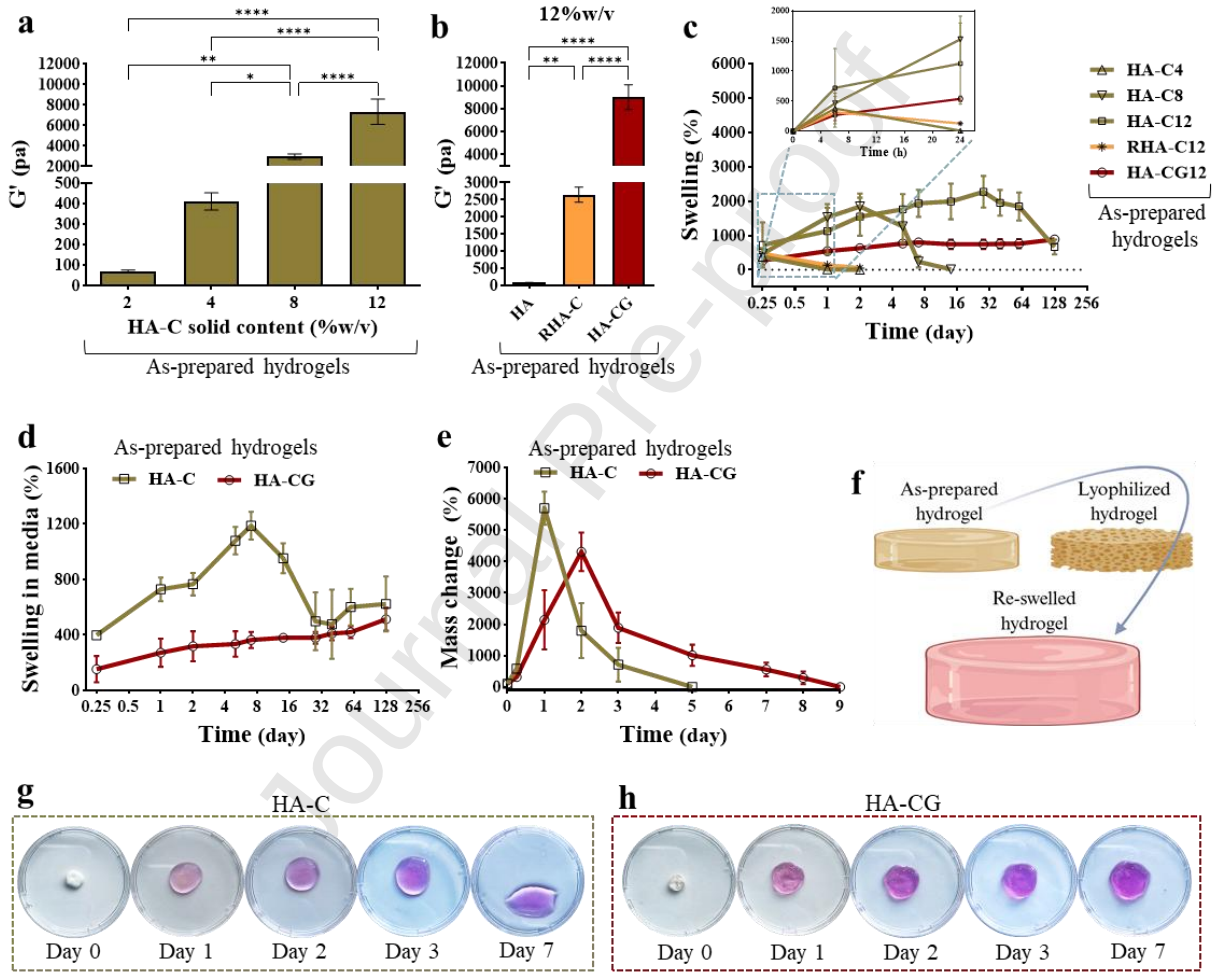

Figure 2. Influence of solid content variation and crosslinking type on the rheological and swelling properties of hyaluronic acid (HA) hydrogels. a) Storage modulus (G′) of HA-C (hydrazide-modified HA) with different solid contents (2–12%) at 1% strain in amplitude sweep measurements. b) G′ of unmodified HA, RHA-C (terminally reduced HA modified with hydrazide), and HA-CG (hydrazide- and gallic acid derivative–modified HA) formulations, all at 12% solid content. c) Swelling ratios of all formulations in PBS at 37 °C. d) Swelling profiles of HA-C and HA-CG (12% solid content) in cell culture medium at 37

°C. e) Enzymatic degradation of HA-C and HA-CG (12% solid content) in hyaluronidase solution at 37 °C. f) Schematic illustration of preparing freeze-dried hydrogel patches and their subsequent reswelling in cell culture medium. g-h) Representative digital images showing reswelling behavior of freeze-dried HA-C and HA-CG samples in cell culture medium, respectively. Statistical analysis: ordinary one-way ANOVA with ****P < 0.0001, ***P < 0.001, **P < 0.01, and *P < 0.05.

One of the important features of such hydrogels is that it is quite easy to produce and are moldable into various desired shapes and dimensions, offering mechanical flexibility and the ability to conform to complex wound geometries. Additionally, these gels can be lyophilized to form dry, porous scaffolds that can serve as wound dressing patches. Depending on the clinical need, these formulations can be adapted for use as band-aids, moist wound dressings, or bandages for larger wound areas with stretchability (Figure 3a). This versatility allows the hydrogels to accommodate different wound types, sizes, and healing phases, making them highly adaptable platforms for personalized wound care. Figure 3b demonstrates the lap shear strength of HA-C (4.8±1.9 kPa) and HA-CG (8.7±2.6 kPa) when applied onto the moist porcine skin models, indicating that when the GA groups were present in the system, the adhesion properties increase significantly. Additionally, Figure 3c presents an ex vivo experiment where an 8 mm wound was created on porcine skin and subsequently filled with lyophilized hydrogel scaffolds. Upon addition of 100 µL of PBS to simulate wound exudate, the scaffolds effectively absorbed the fluid while remaining securely in place. When the skin samples were mechanically twisted at various angles, both HA-C and HA-CG gels maintained their position. However, under submersion and torsion in an aqueous environment, the HA-C gel eventually detached from the tissue, while the HA-CG gel remained firmly adhered. This superior adhesion of HA-CG is likely attributed to the GA derivatives present in the formulation, which are known to display superior tissue adhesive properties than conventional catechol functionalized materials [32]. Such adhesion can be attributed to covalent interactions between the GA moieties and tissue surface proteins having free amino groups, as well as through hydrogen bonding and hydrophobic interactions [33]. This property highlights the potential of HA-CG as a robust and adhesive wound dressing, especially in dynamic or moist environments.

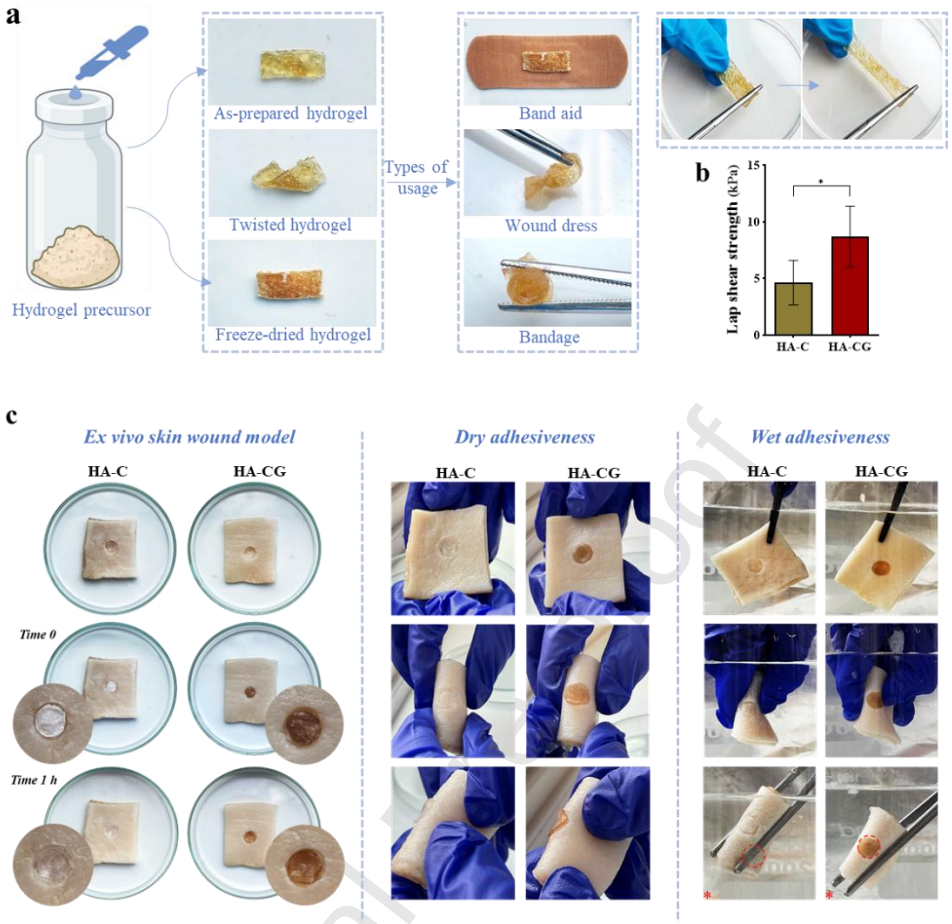

Figure 3. Applications and adhesiveness of hyaluronic acid (HA)-based hydrogel patches. a) Schematic illustration of HA-CG (hydrazide- and gallic acid–modified HA) hydrogel dressing formation, along with digital images demonstrating its versatility. HA-CG can be fabricated into different geometries (e.g., rectangular), bent, twisted, or freeze-dried, enabling use as a band-aid, wet wound dressing, or hydrogel bandage. The hydrogel in its hydrated state also exhibits high stretchability. b) Quantitative adhesiveness of HA-C and HA-CG hydrogels to wet porcine skin through the lap shear test. c) Adhesiveness of HA-C and HA-CG hydrogels to porcine skin after placement into a defect, with representative images showing adhesion under both dry and wet conditions. The red circles in the images marked with red stars indicate the gel position.

2.2. In vitro biological characterization of modified HA

To evaluate the biocompatibility of the HA-C and HA-CG polymers on human mesenchymal stromal cells (hMSCs), varying concentrations of both reagents (0.01, 0.1, 1, and 2 mg/mL) were added to the cell culture media. After 24 h of incubation, Live/Dead staining was performed, with viable cells visualized in green and dead cells in red. As shown in Figure 4a, cells remained highly viable across all concentrations and for both formulations, with only minimal numbers of dead cells observed at higher concentrations. To

quantitatively assess the metabolic activity of the cells, the PrestoBlue assay was conducted. Interestingly, all tested concentrations for both HA-C and HA-CG maintained metabolic activity levels above 90% when normalized to untreated control cells (Figure 4b). However, a slight decrease in metabolic activity was observed at the highest concentration (2 mg/mL), particularly for HA-CG. This reduction is likely attributable to the increased viscosity of the HA-CG solution at higher concentrations, which is expected to have a mild effect on cell metabolism. In addition, an extract cytotoxicity assay according to ISO 10993-5 was performed to assess the biocompatibility of the fully formed hydrogels (Supporting Information, Figure S3). HA-C and HA-CG hydrogels were incubated in complete cell culture medium, and the resulting extracts were subsequently evaluated using a PrestoBlue metabolic activity assay. Cells cultured in standard complete medium served as the control group. The results demonstrated high cell viability (>90%) in all extract-treated groups, indicating that the hydrogels did not release cytotoxic components during incubation. These findings further confirm the cytocompatibility of the fully formed hydrogel networks and complement the direct cell culture experiments performed with the polymer solutions.

Additionally, radical scavenging and intracellular ROS, which play a critical role in various physiological processes, including antimicrobial defense, platelet activation, and angiogenesis, were evaluated. Excessive ROS level is known to cause oxidative stress, which disrupts the wound healing cascade and contributes to chronic inflammation and impaired tissue repair [34]. To evaluate the ROS-scavenging potential of HA-C, HA-CG, and unmodified HA (as a control), we conducted the 2,2′-Azino-bis(3-ethylbenzothiazoline-6-sulfonic acid) diammonium salt (ABTS) radical scavenging assay at a polymer concentration of 1 mg/mL. As shown in Figure 4c, both HA-C and HA-CG demonstrated significant radical scavenging activity (more than 90%), while unmodified HA exhibited minimal activity (less than 10%). The antioxidant activity observed for HA-C is likely attributed to the presence of the hydrazide group, which is known for donating electrons and acting as a radical scavenger [35]. Although the antioxidant activity of hydrazide-modified HA has not been previously reported, related studies, such as those by Bouledb et al., have shown that hydrazone and hydrazide derivatives possess radical scavenging potential, with the NH groups of hydrazones being more reactive than those of hydrazides [36]. In the case of HA-CG, the enhanced radical scavenging is further supported by the presence of GA derivatives, which are well-known for their potent antioxidant properties. As shown in our previous work, GA moieties grafted onto the HA backbone can readily neutralize ROS through hydrogen or electron donation, reinforcing the antioxidant capacity of the hydrogel system [23,29]. Additionally, when the same ABTS assay was performed on the as-prepared hydrogel formulations, similar results were observed with both HA-C and HA-CG gels exhibiting their radical scavenging activity (Supporting Information, Figure S4).

To evaluate the effect of HA-C and HA-CG polymers on intracellular ROS levels, oxidative stress was induced in human dermal fibroblasts (HDFs) by treatment with H_2O_2, thereby elevating intracellular ROS. Following induction, cells were treated with either HA-C or HA-CG. A group of cells treated with H_2O_2 alone served as the positive control, while untreated cells (without H_2O_2) were used as the negative control. Intracellular ROS levels were assessed using dichlorodihydrofluorescein diacetate (DCFDA) staining, which fluoresces green upon oxidation, enabling visualization of ROS accumulation. As expected, the positive control group exhibited strong green fluorescence, indicating elevated ROS levels, while the negative control group showed minimal fluorescence. Remarkably, cells treated with HA-C or HA-CG displayed significantly reduced fluorescence intensities, comparable to the negative control, indicating a substantial reduction in intracellular ROS levels (Figure 4d). In addition to intracellular ROS measurements, cell viability under oxidative stress was assessed using the PrestoBlue assay. As shown in Figure 4e, treatment with H_2O_2 alone (positive control) significantly reduced cell viability, with only ~50% of cells surviving the induced oxidative stress. In contrast, treatment with the gel components improved cell survival. Specifically, cells treated with HA-C showed a viability of $64 \pm 8\%$, while HA-CG treatment further enhanced cell viability to $86 \pm 6\%$, indicating a more effective protective effect when GA derivatives were present. To evaluate the contribution of GA moieties alone, an additional group was included in which HA was solely modified with the GA derivative (HA-G). In this group, cell viability reached $70 \pm 6\%$. These findings demonstrate that both hydrazide and GA derivatives have an inherent ability to mitigate oxidative stress. However, their combination in HA-CG provides synergistic antioxidant effects, resulting in superior cellular protection. These results confirm the antioxidant activity of both hydrogel formulations, highlighting their potential to mitigate oxidative stress and suggesting possible anti-inflammatory effects beneficial for wound healing applications.

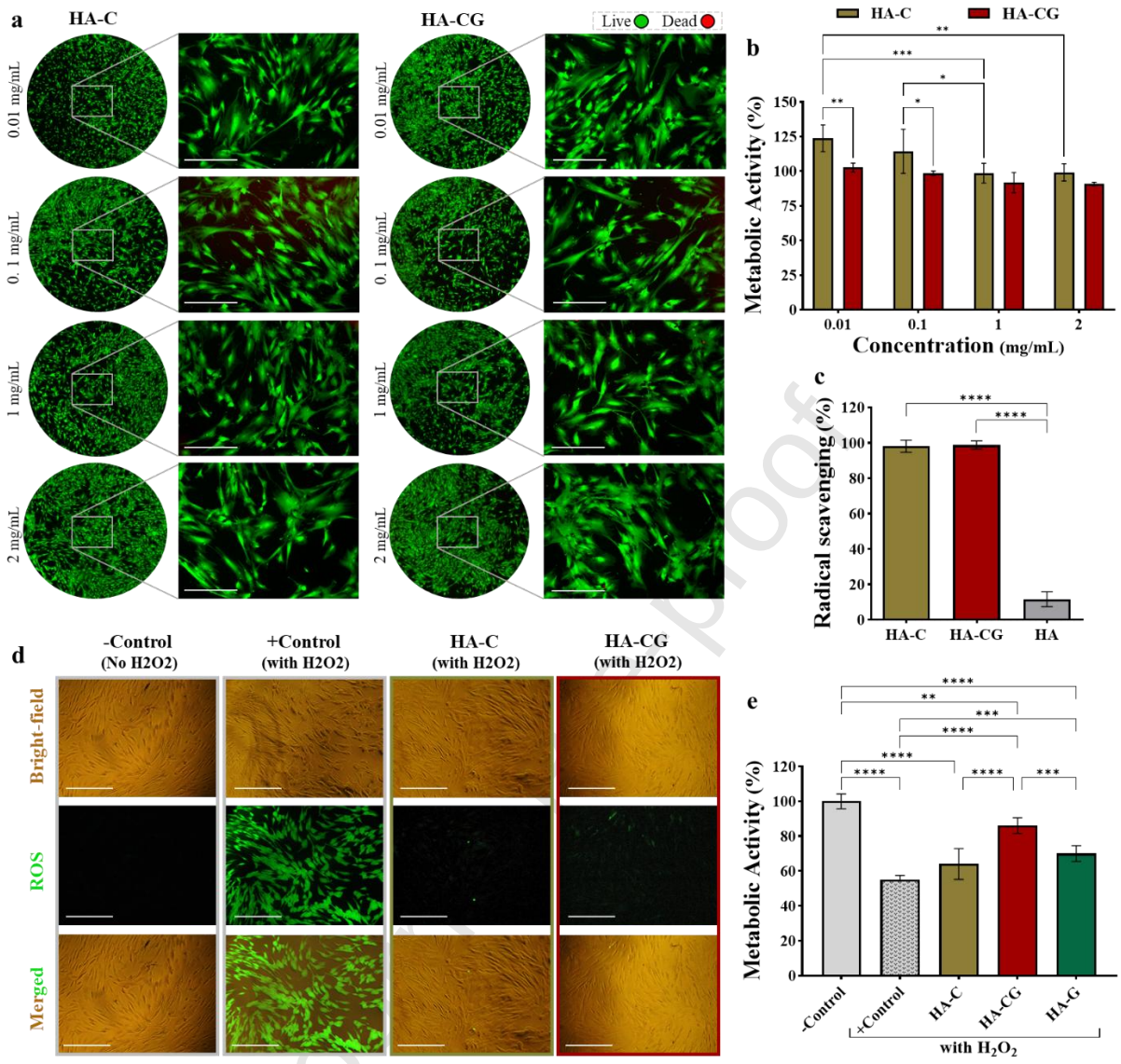

Figure 4. Effect of hydrogel formulations on cell viability and oxidative stress. a) Representative Live/Dead stained images of human mesenchymal stromal cells (hMSCs) cultured with different concentrations of hydrazide-modified HA (HA-C) and hydrazide-plus gallic acid derivative–modified HA (HA-CG). Images were captured at both 2× and 10× magnifications. b) Metabolic activity of hMSCs after 3 days of incubation with HA-C and HA-CG at different concentrations, assessed by PrestoBlue assay. c) Radical scavenging activity of unmodified HA, HA-C, and HA-CG determined by ABTS assay. d) Representative fluorescence microscopy images of intracellular reactive oxygen species (ROS) in human dermal fibroblasts (HDFs), visualized using DCFDA staining. e) Metabolic activity of HDFs under H_2O_2-induced oxidative stress, and the protective effect of hydrogels on cell viability. Scale bar = 150 μm.Statistical analysis: ordinary one-way ANOVA and 2-way ANOVA with ****P < 0.0001, ***P < 0.001, **P < 0.01, and *P < 0.05.

2.3. *Immunomodulatory potential of hydrogel compounds*

Chronic wounds are often marked by sustained inflammation and impaired re-epithelialization [37]. While the immune response is essential for orchestrating wound healing, prolonged or excessive inflammation can significantly hinder tissue regeneration [38]. The present platform is designed as a cell-free wound healing patch, where the therapeutic effect is expected to arise primarily from the gradual degradation of the hydrogel matrix and the release of bioactive polymer-derived components into the wound microenvironment. During in vivo degradation, the hydrogel progressively softens and releases soluble polymer fragments/gel precursors, which may interact with infiltrating immune cells and contribute to the observed immunomodulatory response. Therefore, the in vitro immunomodulation experiment using polymer solutions is designed to assess the biological activity of these soluble components rather than to directly reproduce the mechanical characteristics of the intact 12% hydrogel patch.

To comprehensively evaluate the immunomodulatory potential of the developed hydrogels, three different macrophage-related cell types were employed, namely undifferentiated human monocytic THP-1 cells, THP-1-derived resting macrophages (M0) following (phorbol myristate acetate) PMA stimulation, and activated pro-inflammatory macrophages (M1) obtained by subsequent lipopolysaccharide (LPS) and interferon-gamma (IFN-γ) treatment (Figure 5a). For all the evaluations, the statistical analyses are presented in a format of tables in Supporting Information, Table S2-13.

Blood-derived monocytes are among the first immune cells to arrive at the wound site, where they can differentiate into pro-inflammatory (M1) or anti-inflammatory (M2) macrophages, depending on environmental cues. To assess whether our hydrogel compounds could influence macrophage polarization, we treated human monocytic THP-1 cells with the polymers for 1, 3, and 5 days in the absence of external immunomodulatory agents or differentiation factors. In this study, HA-C and HA-CG were added to the cells, and also solely HA modified with GA derivative (HA-G) was considered here as one of the study groups to investigate the role of GA alone as well. Untreated cells served as the control group. We observed that the expression of IL-10, a key anti-inflammatory cytokine involved in immune regulation and tissue homeostasis, was similar across all groups at day 1 (Figure 5b). However, by day 3, IL-10 levels significantly increased in HA-G (2.6-fold) and HA-CG-treated cells (2.8-fold), suggesting an early shift toward an anti-inflammatory phenotype. By day 5, IL-10 levels declined in the control and HA-C groups, while HA-G and HA-CG groups displayed sustained expression. TGF-β, another immunosuppressive cytokine crucial for tissue remodeling and repair, showed a mild upregulation in the HA-CG group at day 3. By day 5, TGF-β expression was increased in all treatment groups (HA-C, HA-G, HA-CG), but most prominently in the HA-CG (1.4-fold) group. In contrast, expression in the control group declined significantly to 0.15. This may be attributed to the role of HA in stimulating TGF-β signaling and regulating inflammation and enhancing tissue remodeling [39,40]. We also tested the expression of pro-inflammatory

markers. Interestingly, the expression of TNF-α, a key pro-inflammatory cytokine, was unchanged at day 1 but increased moderately at day 3 in the HA-G and HA-CG groups. By day 5, TNF-α levels increased significantly in the control and HA-C (50.3-fold) groups but enhanced more modestly in HA-G and HA-CG, indicating a less inflammatory response in these two groups with GA moieties. Similarly, IL-1β, a pro-inflammatory cytokine, displayed a significant upregulation at day 3 in HA-G (23.2-fold) and HA-CG (26.6-fold). However, the IL-1β expression remained unchanged in the control and HA-C groups. Together, these results demonstrate a dual-phase response in the GA-containing polymers (HA-G and HA-CG). The HA-G and HA-CG polymers induce a transient upregulation of pro-inflammatory markers, followed by a sustained rise in anti-inflammatory cytokines, such as IL-10 and TGF-β. The early induction of IL-10 and TGF-β, coupled with the downregulation of IL-1β by day 5, supports our hypothesis that incorporating GA-derived matrices facilitates a favorable immunomodulatory environment by aiding immune cell recruitment during the early phase of healing, followed by a shift toward the M2 macrophage phenotype, which is essential for resolving inflammation and supporting tissue regeneration [41].

Next, we evaluated how macrophages in the resting state (M0) would respond to the modified HA polymers. Specifically, we investigated the macrophage polarizing capabilities of HA-G, HA-C, and HA-CG polymers over an extended period, specifically at days 1, 3, 5, 7, and 10. As shown in Figure 5c, IL-10 was gradually upregulated over time in groups treated with HA-G and HA-CG, with the highest expression observed at day 10 by 81.3 and 112.9 times increase, respectively. HA-C also induced a mild increase in IL-10 expression, but to a significantly lesser extent. Notably, the untreated control group exhibited minimal change in IL-10 levels throughout the time course. This sustained IL-10 production in the HA-G and HA-CG groups suggests a prolonged anti-inflammatory response, supporting the notion that these materials promote macrophage polarization toward the M2 phenotype [41]. The GA grafted polymer (HA-G and HA-CG) displayed high TGF-β expression, a similar response to IL-10, validating the anti-inflammatory characteristics of GA grafted polymers. Interestingly, unlike IL-10, the highest expression of TGF-β was observed in the HA-C group, relative to HA-G and HA-CG; however, the control group did not show any response. This suggests that the material interactions, particularly those involving HA and the CD44 receptor, play a key role in modulating TGF-β signaling. These results align with the monocyte (THP-1) data, reinforcing our hypothesis that GA-functionalized HA gels potentially promote a wound-resolving characteristic. Regarding TNF-α, we observed only a mild increase at day 7 in all treated groups. However, by day 10, expression levels diverged significantly: the control group showed a robust (17.6-fold) increase, while HA-C and HA-G treated cells showed a restrained increase (3.7-fold), and HA-CG showed a moderate elevation (7.9-fold). This suggests that while some level of mixed immune signaling emerges at later time points, the untreated macrophages develop a strongly pro-inflammatory phenotype over time, likely due to the absence of regulatory cues. In contrast, cells exposed to HA-based materials appear to resist a full M1

transition. Similarly, IL-1β showed a transient increase in HA-G and HA-CG groups at day 3 (similar to THP-1 monocyte response), followed by a significant reduction by day 10. In the HA-C and control groups, IL-1β levels peaked later (day 5), and while HA-C-treated cells had a decline by day 10, the control group showed a sustained and significant increase, reflecting a continued pro-inflammatory state in the absence of any immunomodulatory stimulus. These results together demonstrate that HA-G and HA-CG promote a pro-resolving, immunosuppressive macrophage phenotype, as evidenced by sustained IL-10 and TGF-β expression, and reduced pro-inflammatory signaling over time. Although a mixed immune profile emerged in later stages (particularly by day 10), the pro-inflammatory gene expression was markedly lower in treated groups compared to controls. The antioxidant properties of hydrazide and GA derivatives, combined with the HA-CD44 axis and potential reactive group interactions, may create a favorable microenvironment that actively shifts macrophages toward an M2-like phenotype, even in the absence of external differentiation signals.

Finally, to validate the promising immunosuppressive activity of the polymers, it was critical to assess the cytokine response under inflammatory conditions, mimicking chronic wounds. For this, pro-inflammatory (M1) macrophages were treated with HA-C, HA-G, and HA-CG, and their cytokine expression was monitored over 1, 3, 5, and 7 days. As shown in Figure 5d, treatment with HA-G and HA-CG resulted in a consistent, gradual increase in IL-10 expression, peaking at day 7 with approximately a 12-fold increase in both groups. HA-C also demonstrated an upward trend, though with a slower rate, reaching a ~3-fold increase by day 7. These data highlight the potent immunosuppressive effect of GA derivatives, which is further enhanced when combined with hydrazide groups. Similarly, TGF-β expression increased across all groups at day 3. However, while the control group showed a decline thereafter, HA-G and HA-CG maintained or even further elevated TGF-β levels up to day 7. HA-C showed a moderate increase over time, suggesting both components individually support TGF-β upregulation, but their combination in HA-CG yields a more pronounced effect. TNF-α expression showed a mild rise in all groups at days 3 and 5. However, by day 7, its level significantly decreased in HA-CG, while remaining constant in HA-C and HA-G, and increasing markedly in the control. Interestingly, IL-1β expression remained unchanged in HA-G, steadily increased in HA-C (1.6-fold) and the control group (1.6-fold), but showed a progressive decline in HA-CG (0.17-fold), reaching its lowest level at day 7. This strongly suggests the synergistic anti-inflammatory capacity of HA-CG in dampening key inflammatory mediators.

These findings highlight the significant immunomodulatory potential of HA-CG, particularly in downregulating chronic inflammatory responses in M1 macrophages. While HA-G demonstrated substantial anti-inflammatory effects, likely due to the antioxidant and radical-scavenging capacity of GA derivatives, and HA-C showed moderate effects attributed to hydrazide groups, the combination of both in HA-CG led to superior outcomes. The sustained upregulation of IL-10 and TGF-β in HA-CG-treated M1

macrophages suggests a shift toward a more anti-inflammatory, M2-like phenotype that may promote tissue repair and resolution of inflammation. However, further studies involving protein-level characterization and pathway-specific analyses will be necessary to elucidate the mechanisms underlying the observed immunomodulatory response fully. In particular, flow cytometric analysis of surface markers such as CD86 (M1) and CD206 (M2), together with ELISA-based quantification of secreted cytokines, will be important next steps to confirm the transcriptional changes reported here at the protein level. Nevertheless, the suppression of pro-inflammatory cytokines at the mRNA level, including TNF-α and IL-1β highlights the potential of HA-CG to modulate inflammatory processes associated with chronic wounds. Taken together, these findings suggest that HA-CG possesses a dual function. In addition to serving as a structurally stable antioxidant hydrogel, it exhibits immunomodulatory activity by influencing macrophage-associated inflammatory gene expression, particularly under pro-inflammatory conditions.

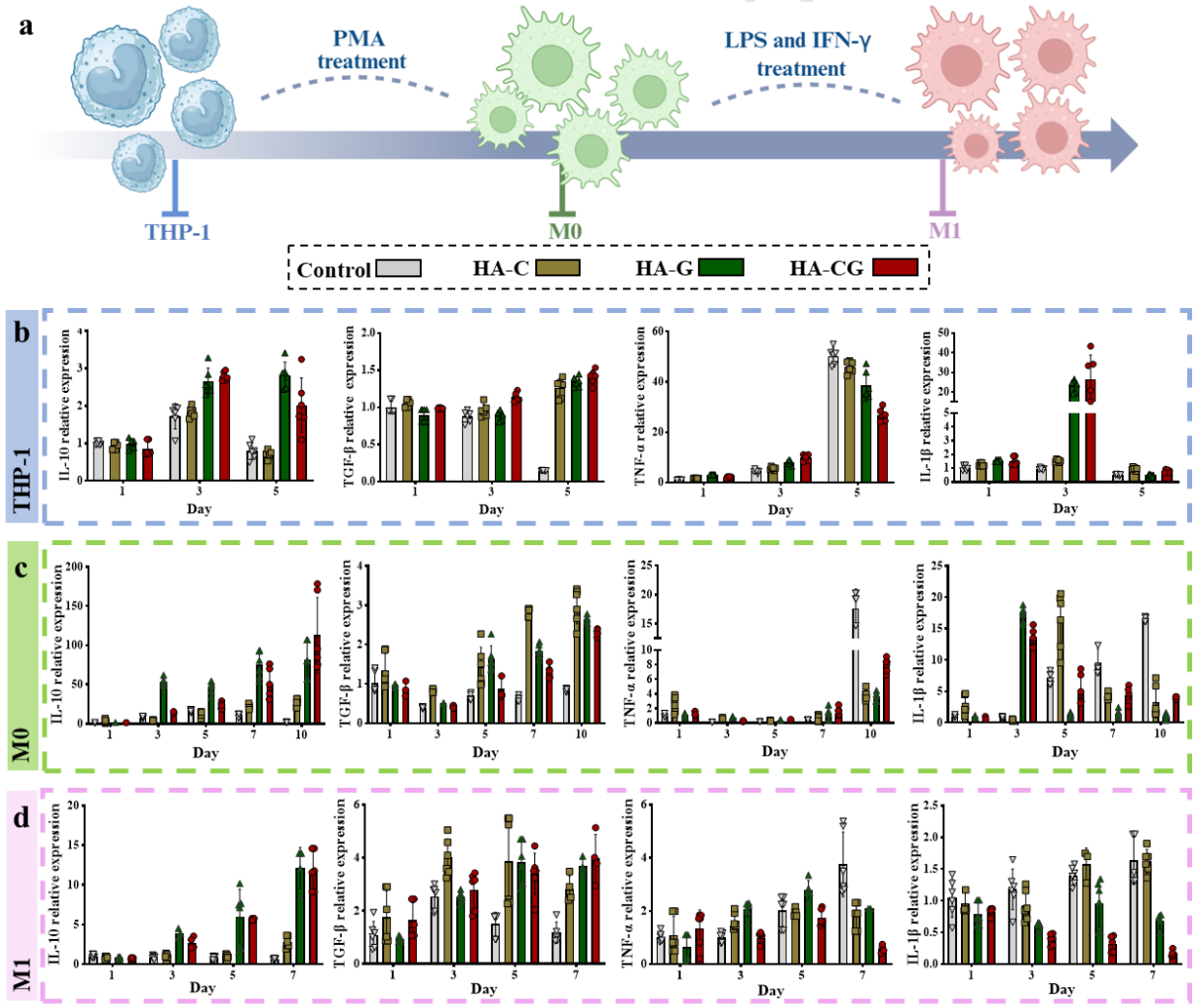

Figure 5. Effect of different hyaluronic acid (HA)-based formulations on immune cell behavior. a) Schematic illustration of differentiation of THP-1 cells into macrophages and their subsequent polarization. b) Effect of different polymer formulations, including hydrazide-modified HA (HA-C), gallic acid–

modified HA (HA-G), hydrazide- and gallic acid–modified HA (HA-CG), and untreated control, on THP-1 cells at days 1, 3, and 5. c) Response of M0 macrophages treated with HA-C, HA-G, and HA-CG formulations at days 1, 3, 5, 7, and 10. d) Effect of hydrogel formulations on macrophages polarized to the M1 phenotype at days 1, 3, 5, and 7. Statistical analysis: 2-way ANOVA with ****P < 0.0001, ***P < 0.001, **P < 0.01, and *P < 0.05. The summary of statistical analysis is presented in the format of a table in the supporting information.

2.4. *Hemostatic and in vivo evaluation of wound healing*

Before evaluating our developed biomaterials for wound healing, we performed a preliminary in vivo evaluation to assess the hemostatic performance of HA-based formulations using a rat liver bleeding model in comparison with a commercially available wound dressing (ChitoTech). The untreated group was used as the control. As illustrated in Figure 6a, a standardized vertical incision was made on the liver surface of the animal model, followed by immediate application of the respective wound dressings. A filter paper was placed over the dressing to absorb excess blood and enable quantitative assessment of blood loss. As shown in the quantitative results (Figure 6b) and visual documentation over time (Figure 6c), both of our scaffold formulations (HA-C and HA-CG) demonstrated superior bleeding control with 177 and 134 mg mass bleeding, respectively, when compared to the control group (324 mg) and even ChitoTech (257 mg). This enhanced hemostatic effect can be attributed to the porous architecture and high fluid-absorption capacity of our hydrogels (as confirmed by swelling studies), together with the known hemostatic effect of adhesive HA [42]. Notably, HA-CG exhibited the most effective hemostasis among all groups. This is consistent with previous studies reporting that the incorporation of GA derivatives enhances the procoagulant and hemostatic properties of wound dressings, likely due to their astringent nature, tissue-adhesive properties, and ability to promote clot formation [43].

Next, we assessed the therapeutic efficacy of HA-C and HA-CG scaffolds as a wound dressing material and compared them with the commercially available wound dressing (ChitoTech). A full-thickness splinted excisional wound model was used as a negative control group. To establish the chronic wound environment, full-thickness subcutaneous defects were created on the dorsal surface of healthy rats by making 1 cm diameter circular wounds. A silicone disc barrier was then placed over each wound to prevent natural closure for 7 days. The wounds were treated for 3, 7, and 14 days with the respective dressings to evaluate their potential in accelerating wound closure and improving overall healing outcomes (Figure 6d).

To assess the therapeutic impact of the different dressings, we monitored the progression of wound healing by photographing the wound beds at baseline (day 0, immediately after wound induction) and on days 3, 7, and 14 following treatment (Figure 6e). The wound areas were measured quantitatively using ImageJ software. As shown in Figure 6f, all groups exhibited a gradual reduction in wound size over time; however, by day 7, the HA-C and HA-CG dressings had already achieved full superficial wound closure, while wounds in the ChitoTech and untreated control groups remained partially open, highlighting the superior

regenerative capacity of our HA-based formulations. At the end of the 14-day treatment period, wounds in the control group were still incompletely healed (~7% open), whereas all treated groups showed complete closure. Interestingly, in the control group, the reduction in wound area did not show a statistically significant difference between Day 7 and Day 14, suggesting a plateau in the healing process during this period. In contrast, all treatment groups exhibited continued and steady wound closure progression up to Day 14. We believe the observed wound-healing could be attributed to the known benefits of HA hydrogels, which are further augmented through their ROS-scavenging properties and anti-inflammatory activity, enabling a faster resolution of chronic wounds compared with the control group. Moreover, the enhanced moisture-retention and fluid-absorption capabilities of HA-C and HA-CG scaffolds likely played an important role as well in accelerating tissue repair.

Key indicators of wound healing, including re-epithelialization and granulation tissue formation, were assessed through histological evaluation using hematoxylin–eosin (H&E) and Masson's trichrome staining. As shown in Figure 7a, H&E staining demonstrated the development of a homogeneous epidermis in all groups. Notably, in the HA-C and HA-CG treatment groups, a more distinct volcano-like morphology was observed at day 7, reflecting the inward contraction of newly formed tissue from the wound edges. At day 14, numerous hair follicles had regenerated in these groups, whereas such structures were absent in the control and ChitoTech groups. In the untreated control group, the wounds displayed features of a markedly thickened epidermis (149 ± 35 μm at day 7), which only partially regressed to 105 ± 21 μm by day 14 (Figure 7b). In contrast, HA-CG treatment promoted early vascularization, as evidenced by the presence of blood cells and angiogenesis as early as day 3 (Figure 7a). By day 14, HA-CG wounds exhibited a markedly thinner epidermis (48 ± 9 μm), approaching the morphology of healthy skin and suggesting more advanced tissue maturation and remodeling. Similar observations have been reported for wound treatments incorporating gallic acid derivatives and extracellular matrix-associated components, which promote improved tissue regeneration and remodeling [8,44].

Granulation tissue formation is another hallmark of the proliferative phase of wound healing, characterized by the activity of fibroblasts, keratinocytes, and endothelial cells, alongside enhanced ECM deposition [45]. As shown in Figure 7c, by day 14, the control and ChitoTech groups exhibited minimal granulation tissue layer formation, measuring 0.68 ± 0.1 mm and 0.71 ± 0.06 mm, respectively. Treatment with the HA-C dressing resulted in a modest improvement (0.94 ± 0.1 mm), while the HA-CG dressing induced the most robust response, forming the thickest granulation tissue of all groups (1.1 ± 0.16 mm). Notably, both HA-treated groups, particularly HA-CG, displayed a higher density of fibroblasts, newly formed blood vessels, and skin appendages such as hair follicles and sebaceous glands compared to the other groups. These features indicate the establishment of a well-organized epidermal and dermal structure closely resembling

mature skin. This outcome likely arises from the intrinsic ability of HA to support skin remodeling, combined with the anti-inflammatory capacity of HA-CG, which can suppress inflammation and thereby promote tissue remodeling and accelerated repair in hard-to-heal wounds.

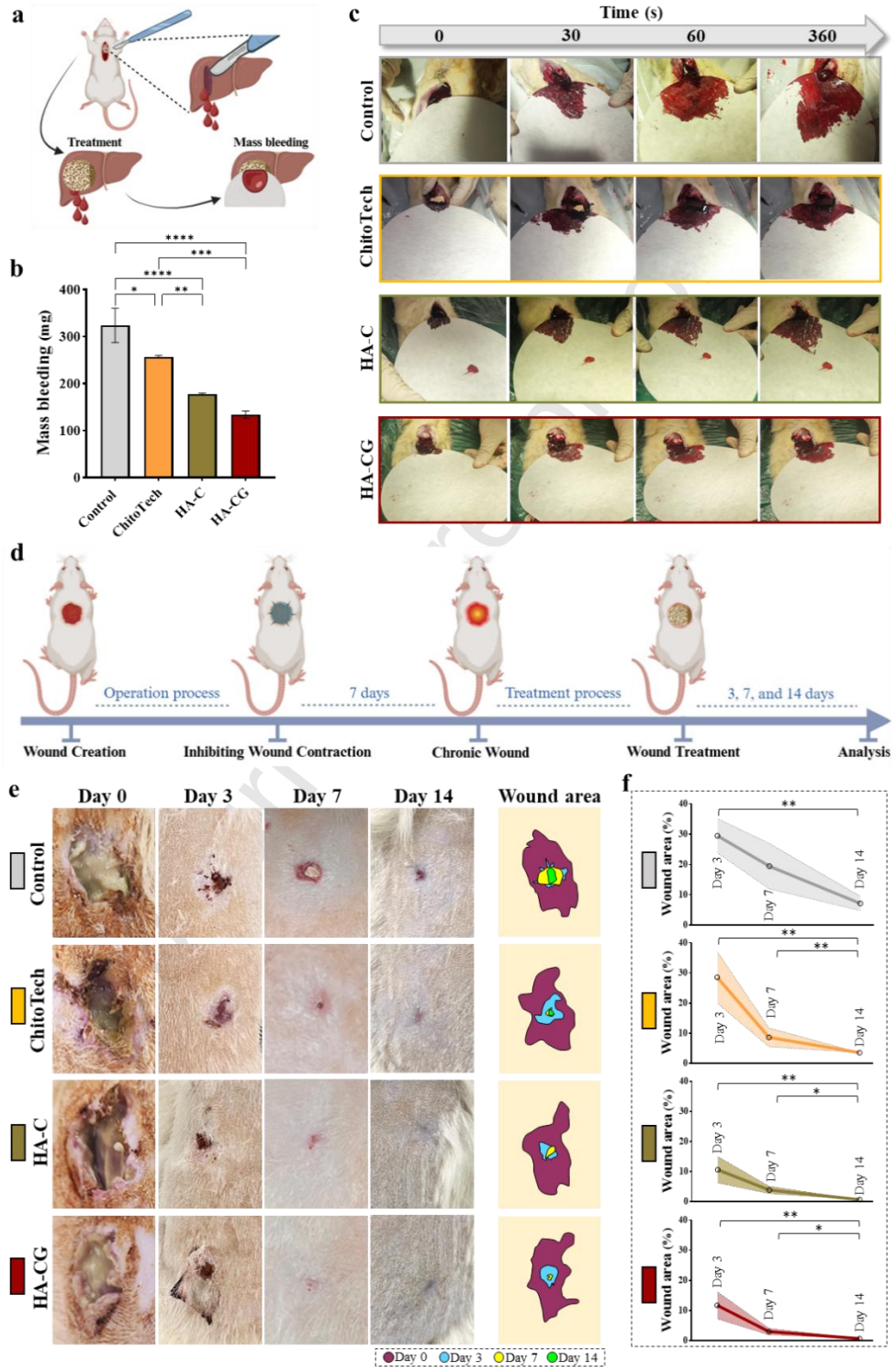

Figure 6. Hemostatic and wound healing capacity of hyaluronic acid (HA)-based formulations. a) Schematic illustration of the hemostatic process in a rat liver bleeding model. b) Quantitative data of total blood loss measured by the weight difference of pre- and post-bleeding filter papers. c) Representative digital images of bleeding sites captured at different time points after injury. d) Schematic illustration of the animal wound model, including wound creation, induction of a full-thickness splinted excisional wound model by delaying closure for 7 days, and subsequent treatment. e) Representative digital images of wound healing progression over 14 days in groups treated with PBS (control), a commercial wound dressing (ChitoTech), HA-C (hydrazide-modified HA), and HA-CG (hydrazide- and gallic acid–modified HA). f) Quantitative wound area reduction over time, calculated from digital images using ImageJ software. Statistical analysis: ordinary one-way ANOVA (n=3) in comparison with ****$P < 0.0001$, ***$P < 0.001$, **$P < 0.01$, and *$P < 0.05$.

We further investigated collagen deposition in the newly formed tissue, as it plays a crucial role in enhancing the tensile strength of neo-tissue during the later stages of wound healing. Therefore, the extent and organization of collagen deposition serve as important indicators of wound repair quality [46]. To assess this, Masson Trichrome staining was performed to visualize collagen architecture (Figure 7d). In the control group, collagen bundles appeared thickened, irregular, and uneven as early as day 3. While increased collagen thickness may contribute to skin firmness, it often leads to excessive stiffness and raises the risk of scar formation [46]. In contrast, the ChitoTech, HA-C, and HA-CG groups exhibited a more uniform collagen deposition compared to the untreated control group. Among them, the HA-CG group showed the most intense staining, suggesting higher collagen content throughout the 14-day study period (Figure 7d). By day 14, collagen in the HA-CG-treated wounds appeared more organized, with an overall structure resembling that of healthy skin. This enhanced remodeling effect might be attributed to the biological properties of GA moieties, including their potent antioxidant and anti-inflammatory activities [20]. Beyond free radical scavenging, GA also promotes the proliferation and migration of dermal fibroblasts and keratinocytes into the wound bed, thereby accelerating tissue regeneration [47]. Collectively, these findings suggest that HA-CG hydrogel, with its ROS-scavenging and immunomodulatory capabilities, not only accelerates wound closure but also substantially improves the quality of regenerated skin, potentially minimizing fibrosis and scar formation.

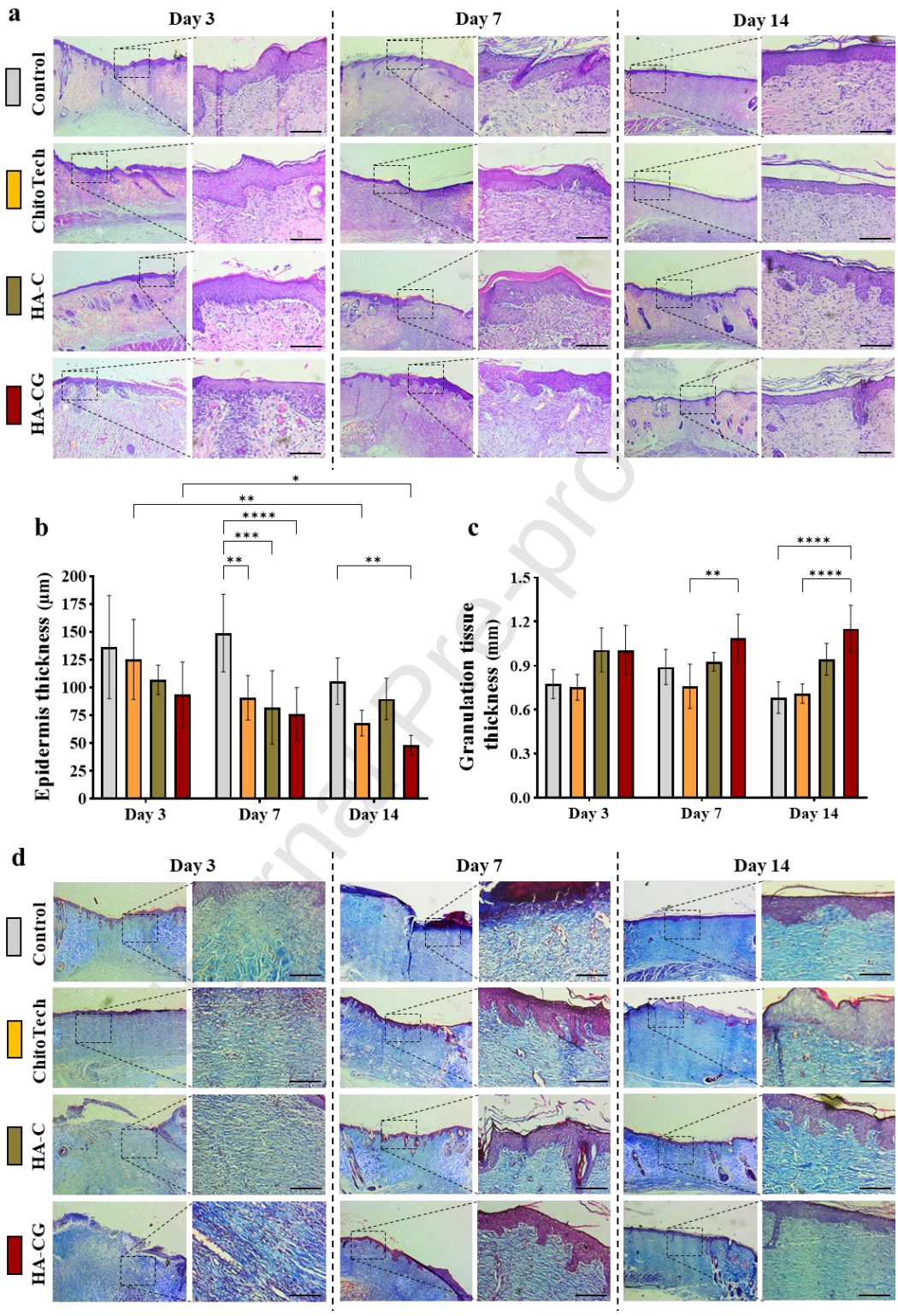

Figure 7. In vivo evaluation of a full-thickness splinted excisional wound model in response to different treatments. a) Representative H&E-stained wound tissue sections and corresponding magnified views from each group on days 3, 7, and 14 post-treatment. b) Quantitative analysis of epidermal thickness across groups, measured using ImageJ software. c) Quantification of granulation tissue thickness from H&E-

stained sections using ImageJ software. d) Representative Masson's trichrome-stained wound tissue sections and corresponding magnified views from each group on days 3, 7, and 14 post-treatment. Scale bar = 150 μm. Statistical analysis: 2-way ANOVA with ****P < 0.0001, ***P < 0.001, **P < 0.01, and *P < 0.05.

To determine the deposition of type I collagen (COL I) within the granulation tissue, we performed immunohistochemistry (IHC) staining across all treatment groups at days 3 and 14 post-treatment, and the results were quantified (Figure 8a–b). On day 3, all groups exhibited COL I expression exceeding 10%, with a gradual increase observed over time. Notably, in the HA-CG group, the initial deposition at day 3 was slightly lower than in the HA-C and ChitoTech groups. However, COL I levels in HA-CG increased significantly over the treatment period, reaching 31 ± 9% by day 14, higher than all other groups. This trend highlights the superior ability of HA-CG to modulate immune responses, suppress excessive inflammation, and thereby create a more favorable environment for sustained collagen deposition and matrix remodeling. While a controlled inflammatory response is essential for initiating wound healing, excessive or prolonged inflammation can impair repair and contribute to chronic wound pathology. To further investigate the inflammatory status in a full-thickness splinted excisional wound model, TNF-α expression was also assessed by IHC staining (Figure 8c), and the number of TNF-α–positive cells was quantified (Figure 8d). At day 3, the control and HA-C groups displayed stronger TNF-α signals compared with ChitoTech and HA-CG. This finding may reflect the persistence of initial inflammation in untreated wounds and HA-C–treated wounds, whereas the potent anti-inflammatory effect of HA-CG markedly suppressed it at early stages. By day 14, TNF-α expression in the control group continued to rise, indicating progression toward chronic inflammation. In contrast, TNF-α levels in the ChitoTech group remained stable, suggesting partial management of the wound environment and limited regulation of inflammatory signaling. Interestingly, both HA-C and HA-CG significantly reduced TNF-α expression over time, with HA-CG showing the most profound reduction, resulting in the lowest number of TNF-α–positive cells at day 14. These results strongly support the role of GA derivatives in mitigating chronic inflammation by regulating immune responses and ultimately creating a more conducive environment for wound repair. However, further macrophage-specific immunostaining and mechanistic analyses will be required to fully elucidate the in vivo immune-modulatory effects.

Beyond collagen deposition and inflammation control, the establishment of local vasculature is vital for wound repair, as it ensures a continuous supply of oxygen, nutrients, and growth factors. Chronic wounds are often characterized by impaired angiogenesis, making neovascularization a critical step in effective tissue regeneration [46,48]. To evaluate the angiogenic potential of our formulations, capillary density around the wound site was assessed using IHC staining for CD31, a well-established marker of endothelial cells and angiogenesis (Figure 8e). Quantitative analysis (Figure 8f) revealed that the HA-CG–treated group exhibited the highest blood vessel density at both day 3 and day 14. In contrast, the control group displayed

the lowest vessel density, highlighting the compromised angiogenic response in untreated wounds. These findings demonstrate that HA-CG not only accelerates wound closure but also facilitates sustained angiogenesis, which is critical for appendage survival, functional tissue regeneration, and long-term remodeling.

Taken together, these findings suggest that HA-CG exhibits superior therapeutic performance in this wound model, promoting accelerated wound closure, reduced inflammation, and improved tissue regeneration. Nevertheless, the present model does not fully recapitulate the complex pathophysiology of chronic wounds encountered in clinical settings. Therefore, future studies employing more clinically relevant models, including diabetic and infected wound models, as well as long-term safety evaluations, will be necessary to further validate the therapeutic efficacy and translational potential of this hydrogel system.

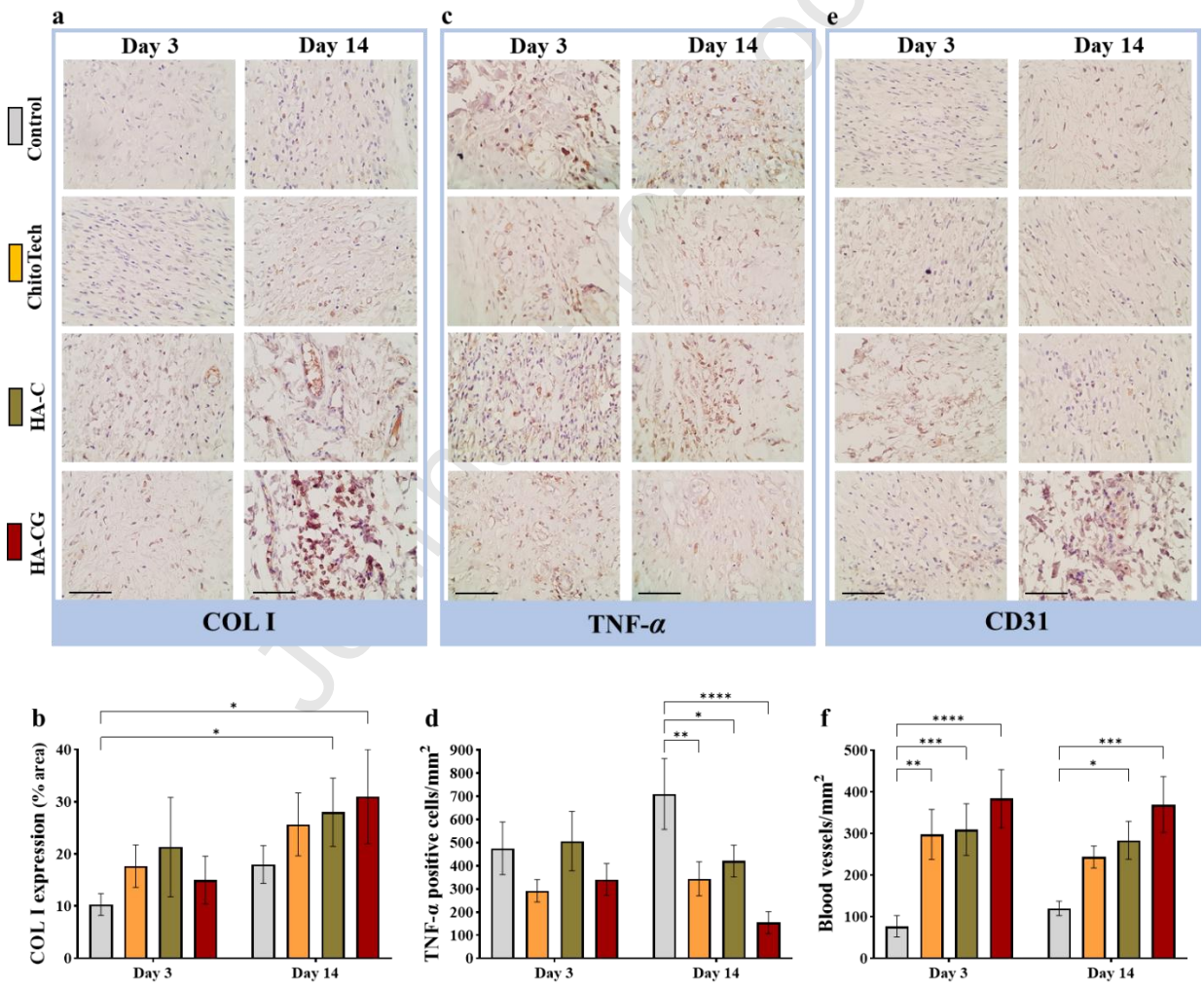

Figure 8. Immunohistochemical (IHC) evaluation of tissue remodeling and inflammatory regulation in a full-thickness splinted excisional wound model following different treatments. a) Representative IHC staining images of collagen type I (COL I) expression in wound tissues on day 14 post-treatment. b) Quantitative analysis of COL I expression from IHC images at day 14. c) Representative IHC staining

images of TNF-α expression in wound tissues on day 14. d) Quantitative analysis of the density of TNF-α-positive cells at day 14. e) Representative IHC staining images of CD31 expression in wound tissues on day 14. f) Quantification of blood vessel density based on CD31 staining at day 14. Scale bar = 100 μm. Statistical analysis: 2-way ANOVA with ****P < 0.0001, ***P < 0.001, **P < 0.01, and *P < 0.05.

3. Conclusion

In this study, we developed a novel HA–based hydrogel patch designed for the treatment of hard-to-heal wounds. The hydrogel was synthesized by simultaneously modifying HA with hydrazide and GA derivative groups, enabling self-crosslinking without the need for a secondary aldehyde-bearing polymer. This design offers significant advantages by providing a user-friendly wound dressing that requires no mixing of separate components, ensuring reproducibility and ease of application. This single-component system simplifies fabrication, eliminates the challenges related to component mixing, and ensures uniform gel formation. The incorporation of GA derivatives enhanced the long-term stability of the hydrogel and equipped it with intrinsic antioxidant activity, effectively protecting cells from oxidative stress. These characteristics also contributed to the immunomodulatory behavior. In vitro studies demonstrated that the dual-modified HA promoted macrophage polarization toward the anti-inflammatory M2 phenotype, while suppressing inflammatory responses in M1 macrophages. Consistently, in vivo experiments confirmed that application of the HA patch with hydrazide and GA moieties on a full-thickness splinted excisional wound model accelerated wound closure, promoted healthy granulation tissue formation, and reduced epithelial thickness, demonstrating improved healing. Furthermore, the patch effectively contributed to a cleaner wound microenvironment.

Overall, this multifunctional hydrogel patch provides a stable, absorbent, and bioactive wound dressing with antioxidant and immunoregulatory properties, offering a promising platform for the treatment of hard-to-heal wounds. Nevertheless, while the present study demonstrates favorable in vitro biocompatibility and promising therapeutic efficacy in vivo, further investigations, including comprehensive biosafety, hemocompatibility, systemic toxicity, and long-term performance assessments, will be required before clinical translation.

4. Experimental section

4.1. Materials

Hyaluronic acid (HA) (MW 200 kDa) was purchased from LifeCore Biomedical (Chaska, USA), 1-ethyl-3-(3-dimethyl aminopropyl)-carbodiimide hydrochloride (EDC), 1-hydroxy benzotriazole hydrate (HOBt), sodium borohydride, and carbodihydrazide (CDH) were purchased from Sigma-Aldrich. Dialysis

membranes used for purification were purchased from Spectra Por (Spectra Por, MWCO 12-14 kDa). All solvents were of analytical quality. Other chemicals used are mentioned in each section in which they were employed.

4.2. Modification of HA with CDH functional groups (HA-C)

The modification of HA with CDH was carried out using carbodiimide coupling chemistry following our previous protocol [23]. Briefly, 1 mmol of HA (400 mg, 1 equivalent) was dissolved in 120 mL of de-ionized water. Thereafter, 1 mmol CDH (90 mg, 1 equivalent) and 1 mmol HOBt (135 mg, 1 equivalent) were added to the aqueous HA solution. The pH of the reaction mixture was adjusted to 4.5 by dropwise addition of 1 M NaOH and 1 M HCl. Finally, 0.3 mmol EDC (57.5 mg, 0.3 equivalent) was added in two batches, and the mixture was stirred overnight. The reaction mixture was loaded into a dialysis bag (MWCO 12-14 kDa) and dialyzed against dilute HCl (pH = 5) containing 50 mM NaCl (4 × 2L, 48 h) and thereafter dialyzed against deionized water (2 × 2L, 24 h). The solution was lyophilized to obtain a white, fluffy material. The degree of hydrazide modification was determined using a trinitrobenzene sulfonic acid (TNBS) assay and UV-VIS-NIR spectrophotometer. Additionally, a control was considered where, during the synthesis, first HA was reduced with 5 mmol of sodium borohydride (189 mg, 5 equivalents), and then CDH was conjugated as described earlier (RHA-C polymer).

4.3. Modification of HA with CDH and GA functional groups (HA-CG)

1 mmol of HA (400 mg, 1 equivalent) was dissolved in 120 mL of deionized water, and later 1 mmol HOBt (153 mg, 1 equivalent) was added. 1 mmol hydrazide derivative of GA (184 mg, 1 equivalent) as synthesized separately was dissolved in 50 ml DMSO, added to the HA solution dropwise, and stirred for 30 min [23]. The pH of the reaction solution was adjusted to 4.5 with 1 M HCl and 1 M NaOH. Then 0.2 mmol EDC (38 mg, 0.2 equivalent) was added, and the mixture was stirred for 6 h. Afterward, the pH was adjusted again to 4.5, and 0.3 mmol EDC (57.5 mg, 0.3 equivalent) and 1 mmol CDH (90 mg, 1 equivalent) were added to the reaction and stirred overnight. The reaction mixture was then loaded into a dialysis bag (MWCO 12-14 kDa) and dialyzed against dilute HCl (pH = 5) containing 50 mM NaCl (6 × 2L, 48 h) and then dialyzed against deionized water (4 × 2L, 24 h). The solution was lyophilized to obtain a white, fluffy solid material.

4.4. Hydrogel preparation

To prepare hydrogels, 2, 4, 8, and 12 mg of HA-C were dissolved in 100 μL of PBS separately, and placed in cylinder molds with 8 mm diameter, the samples named HA-C2, HA-C4, HA-C8, and HA-C12, respectively. Additionally, hydrogels incorporating RHA-C and HA-CG were prepared by dissolving 12 mg of each in 100 μL of PBS. The mixtures were vortexed until a homogeneous viscous solution was formed

and subsequently incubated at 37 °C overnight. For some of the experiments, following incubation, the samples were snap-frozen in liquid nitrogen and freeze-dried.

4.5. Rheological and adhesion characterization of hydrogel

To evaluate the rheological properties of the hydrogels, the stiffness of the prepared hydrogels was assessed in the wet state before the freeze-drying step. Rheological measurements were conducted using a TA Instruments TRIOS Discovery HR 2 rheometer. The storage modulus (G') and loss modulus (G") were determined through an amplitude sweep, and the results were plotted against strain to illustrate the viscoelastic shear behavior of the hydrogels. The G' values at 1% strain were reported for each sample to enable comparison across different groups.

The adhesive properties of the developed hydrogels were quantified using a lap shear test. Briefly, fresh porcine skin was cut into rectangular pieces (30 × 25 mm), and the dermal side of each sample was fixed onto rigid plastic substrates using a low-viscosity cyanoacrylate adhesive (Merck, Sweden). Before hydrogel application, the tissue surface was pre-wetted with PBS to mimic the moist environment of a wound bed. Freeze-dried hydrogel patches were then placed onto one skin surface and rehydrated with PBS, forming a circular adhesive area with a diameter of 20 mm. A second skin sample was subsequently overlapped onto the hydrogel-covered area to create the bonded interface. The assemblies were maintained under gentle contact for 15 min, wrapped in PBS-moistened gauze, and incubated in a humid environment for 1 h before testing. Lap shear measurements were performed using an Instron 5943 universal testing machine equipped with a 50 N load cell. The samples were pulled to failure at a crosshead speed of 5 mm min^{-1}. The maximum force recorded before failure was used to calculate the lap shear strength.

4.6. Swelling measurement and stability of hydrogels

To study the swelling characteristics of the hydrogels, the prepared samples were incubated in PBS (pH 7.4) at 37 °C. Briefly, the samples were placed in glass vials, and their initial weights were recorded. The hydrogels were then submerged in PBS or cell culture media for the swelling study. At each measurement time point, the weight of each gel was recorded, and fresh PBS was added to the vials. The swelling percentage was calculated using equation (1). For stability measurements, the hydrogels were incubated in PBS containing 1 M NaCl or 1 M urea to assess their resistance to these conditions, and also in both acidic and basic conditions.

To assess the degradability potential of hydrogels in hyaluronidase, the samples were kept in hyaluronidase solution (210 U/mL, approximately 35 times the concentration of the enzyme in human plasma) at 37 °C. At each time point, the weight of the samples was recorded, and fresh degradation solution was added. The degradation profile was calculated according to equation (2).

$$Swelling(\%) = \frac{\text{Mesaured weight} - \text{Initial weight}}{\text{Initial weight}} \quad (1)$$

$$Mass\ change\ (\%) = \frac{w_t}{w_0} \quad (2)$$

4.7. Antioxidant assessment

The radical scavenging and antioxidant properties of the samples were evaluated using the 2,2′-Azino-bis(3-ethylbenzothiazoline-6-sulfonic acid) diammonium salt (ABTS) assay. The radical cation ($ABTS^+$) was generated by oxidizing ABTS (7.00 mM) with potassium persulfate (4.95 mM) in a 1:1 volume ratio. The reaction mixture was kept in the dark at room temperature for 16 h. The resulting $ABTS^+$ solution was then diluted with deionized water to achieve an absorbance of 0.70 ± 0.02 at 734 nm, as measured using a UV-VIS microplate reader. To evaluate the radical scavenging activity of the hydrogels, the prepared gels were immersed in 2 mL of $ABTS^+$ solution and incubated in the dark at room temperature for 5 min. For assessing the antioxidant properties of different HA modifications (precursors) and also prepared gels, the samples were added to the $ABTS^+$ solution at a final concentration of 1 mg/mL and incubated under the same conditions. Following incubation, the absorbance at 734 nm was measured, and the ABTS scavenging activity was calculated using equation (3).

$$\text{The ABTS scavenging activity (\%)} = [(A_{control} - A_{sample}) / A_{control}] \times 100 \quad (3)$$

$A_{control}$ represents the absorbance of the blank $ABTS^+$ solution, and A_{sample} denotes the absorbance of the solution in the presence of polymer samples.

4.8. Cell culture

Human mesenchymal stromal cells (hMSCs) were cultured in T-150 cell culture flasks using Dulbecco's Modified Eagle Medium (DMEM, Gibco), supplemented with 10% fetal bovine serum (FBS, Gibco) and 1% antibiotic-antimycotic (AA). The cells were maintained in a cell culture incubator at 37 °C with 5% CO_2. The medium was replaced every two days, and cells were passaged when they reached approximately 80% confluency. Cells from passages 2–6 were used for the experiments.

HDF cells, human dermal fibroblasts, were cultured in T-75 cell culture flasks in DMEM (Gibco), supplemented with 10% FBS and 1% AA. Cells from passages 12–16 were used for the experiments.

THP-1 cells, a human monocytic cell line, were cultured in suspension form in T-25 cell culture flasks using Roswell Park Memorial Institute (RPMI) 1640 medium (Gibco), supplemented with 10% FBS and 1% AA as an antibiotic. The cells were maintained in a cell culture incubator at 37 °C with 5% CO_2. The media was changed every other day, and cells were counted at the same time until the number of cells was enough for further analysis. Cells from passages 13–18 were used for experiments.

4.8.1. Biocompatibility and Live/Dead staining

To analyze the biocompatibility of the samples, hMSCs were seeded in a 24-well plate. After 24 h, once the cells had adhered, they were treated with different concentrations of gel precursors. Various concentrations of HA-C and HA-CG (0.01, 0.1, 1, and 2 mg/mL) were added to the cell culture medium and incubated with the cells for three days. Cells cultured in media without gel precursors were used as the control group. After 3 days, cell viability was assessed using Live/Dead staining (Viability/Cytotoxicity Kit for Mammalian Cells, ThermoFisher). Cells were washed with PBS and incubated with Live/Dead staining solution (containing 1 µL/mL Calcein AM and 2 µL/mL Ethidium homodimer in cell culture medium) for 30 min at 37 °C. Following incubation, cells were washed with PBS and imaged using a Nikon Eclipse Ts2 fluorescence microscope. Image analysis was performed using ImageJ software, and cell viability was calculated by comparing the number of green-stained live cells to the total number of green (live) and red (dead) cells.

In parallel, the metabolic activity of cells treated with different concentrations of HA-C and HA-CG was measured after 3 days of culture using the Presto Blue assay, a resazurin-based viability assay. After 3 days of incubation, cells were washed with PBS and treated with 10% Presto Blue solution (ThermoFisher). The samples were incubated for 4 h, and fluorescence intensity was measured using a plate reader at an excitation wavelength of 555 nm and an emission wavelength of 595 nm.

4.8.2. Intracellular ROS measurement and cell viability under oxidative stress

To assess the influence of gel precursors on cell response under oxidative stress, a DCFDA fluorescence staining assay was performed. For the staining, 15000 HDF cells per well were seeded into a 48-well plate and incubated overnight. Afterwards, cells were incubated with 400 µm H_2O_2 to induce oxidative stress. Following this, gel precursors were prepared at a concentration of 1 mg /mL in culture media. These solutions were added to the cell culture medium, while a separate control group without H_2O_2 treatment was included as a negative control. After 24 h incubation, the medium was aspirated, and the cells were washed twice with PBS. The cells were then incubated in a 10 µm solution of DCFH-DA for 40 min and kept in the dark at 37 °C. DCFH-DA is a cell-permeable, non-fluorescent dye that, in the presence of ROS such as H_2O_2, was oxidized to form dichlorofluorescein (DCF), a highly fluorescent molecule. After

staining, the DCFDA solution was washed out, and the cells were washed twice with PBS. Then, fluorescent images were captured using a fluorescence microscope to assess intracellular ROS levels.

To investigate the viability of cells under oxidative stress, the same condition was considered. Here, after the incubation period, the metabolic activity of cells was measured using Presto Blue assay as explained earlier.

4.8.3. Evaluation of the effect of modified HA polymers on immune cells

THP-1 cells were seeded in 12-well plates at a density of 2×10^5 cells per well. For M0 differentiation, cells were cultured in RPMI complete medium supplemented with 25 ng/mL PMA. After 24 h, round and partially adherent M0-like cells were observed under the microscope, confirming successful initiation of differentiation. To ensure full differentiation, cells were maintained in the same medium for 48 h, by which time the majority had transformed into M0 macrophages. The differentiation medium was then removed, and cells were gently rinsed once with PBS. For M1 polarization, cells were cultured in RPMI complete medium containing 100 ng/mL LPS and 20 ng/mL IFN-γ. Following 48 h of incubation at 37 °C and 5% CO_2, cells exhibited an elongated, adherent morphology characteristic of M1 macrophages, indicating successful polarization.

HA-C, HA-G, and HA-CG polymers were sterilized under UV light for 20 min, transferred into sterile tubes, and dissolved in RPMI complete medium under aseptic conditions. The polymer suspensions were vortexed for 5 min and incubated at 37 °C to facilitate dissolution. Once fully dissolved, the culture medium (control or polarization medium) was removed, and 1 mL of polymer solution was added to each well. A control group treated only with RPMI complete medium was included in parallel. Cells were incubated at 37 °C and 5% CO_2, with media refreshed every 2–3 days according to the time points. To evaluate the anti-inflammatory effects of the polymers, cells were harvested at designated timepoints for RNA isolation and RT-qPCR analysis. At each designated time point, cells were lysed using lysis buffer, and total RNA was extracted with the RNeasy Plus Mini Kit (Qiagen) according to the manufacturer's instructions. cDNA was synthesized from the isolated RNA, and qPCR was performed to evaluate gene expression. For qPCR, cDNA samples were mixed with TaqMan Fast Advanced Master Mix (Thermo Fisher Scientific), nuclease-free water (Invitrogen), and specific TaqMan assay primers. Amplification was carried out on a Bio-Rad CFX96 real-time PCR system following the manufacturer's protocol. The expression of TNF-α, IL-1β, IL-10, and TGF-β was assessed using commercially available TaqMan primers, with GAPDH serving as the internal control. Gene expression levels were normalized to GAPDH and further expressed relative to the mRNA levels of the day 1 control group.

4.9. Hemostatic ability evaluation

The hemostatic performance of the developed hydrogels was evaluated using a rat liver bleeding model (male rats, 200–250 g), as previously reported [49]. All animal procedures were carried out in accordance with the guidelines of the Tehran Heart Center. Briefly, rats were anesthetized with 10% chloral hydrate (5 mg/kg, intraperitoneal injection), and the liver was exposed through a midline abdominal incision. Hemorrhage was induced using an 18 G needle, after which a pre-weighed filter paper was placed beneath the liver to collect blood. The freeze-dried wound dressings were then immediately applied to the bleeding site. Hemostasis was monitored by photographing the wound every 30 s until complete cessation of bleeding. The total blood loss was determined by measuring the change in filter paper weight before and after bleeding. Results were compared with a control group (no treatment).

4.10. In vivo wound healing experiments

To establish the in vivo full-thickness wound healing model, male Sprague–Dawley (SD) rats weighing 300-400 g (Orient Bio, Seongnam, Korea) were used for implantation of wound dressings into subcutaneous tissue. Animals were housed individually at the Heart Institute Center of Tehran in temperature-controlled cages (24 ± 1 °C) with a 12 h light/dark cycle and had free access to standard chow and water. All animal procedures were conducted in accordance with the Guidelines for the Care and Use of Laboratory Animals of Tehran University of Medical Sciences and were approved by the Animal Ethics Committee (Code of Ethics: IR-TUMS.THC.REC.1405.024).

A full-thickness splinted excisional wound model was established based on previously reported methods. Briefly, rats were anesthetized with intraperitoneal injections of ketamine and xylazine. The dorsal hair was shaved, and the skin surface was disinfected with 75% ethanol. Full-thickness circular excisional wounds (1 cm diameter) were created on the dorsum using a sterile biopsy punch. To minimize wound contraction and maintain the wound in an open state, a silicone ring was placed around the wound and secured to the surrounding skin using sutures, following previously reported splinted wound models. After 7 days, rats were randomly assigned to four treatment groups: control (untreated), HA-C hydrogel dressing, HA-CG hydrogel dressing, and a commercially available wound dressing (Chitoheal Foam, Chitotech, Iran). Following anesthesia, treatments were applied to the wounds with gentle pressure for 5 min and then covered with Tegaderm film to secure the dressings. Wounds were photographed on days 0, 3, 7, and 14 using a digital camera, and wound areas were quantified using ImageJ software. Digital images of wounds were collected at predetermined time points, and wound areas were quantified using ImageJ software. Due to the application of a silicone ring barrier to delay wound contraction, the initial wound shapes at Day 0 were not perfectly circular and exhibited some morphological variation. Therefore, wound closure was calculated as the percentage of wound area reduction relative to the corresponding Day 0 wound area for each individual wound

At each experimental time point, rats were euthanized by overdose of chloral hydrate. Excised wound tissues were fixed in 10% formalin, embedded in paraffin, and sectioned for histopathological analysis. Hematoxylin and eosin (H&E) staining and Masson's trichrome staining were performed to evaluate intra-tissue healing and collagen deposition, respectively. For H&E staining, thin tissue sections were incubated with hematoxylin for 5 min, followed by counterstaining with 0.5% eosin for 6 min at room temperature. The sections were then dehydrated through graded ethanol (80% ethanol for 30 s, 95% ethanol for 1 min × 2, and absolute ethanol for 3 min × 2), cleared with xylene, and mounted. The stained slides were imaged using a full-slide scanner (Zeiss AxioScan.z1, Japan). Quantitative analysis of neo-epithelial length was performed using ImageJ software. Granulation tissue thickness was also quantified using ImageJ software. In this regard, the upper boundary was defined as the interface between the newly formed epidermis and the underlying granulation tissue, while the lower boundary was defined as the transition between the granulation tissue and the underlying dermis/subcutaneous tissue. Measurements were performed at multiple locations across the wound bed and averaged for each sample.

To evaluate collagen deposition in granulation tissue, Masson's trichrome staining (Solarbio, G1340) was conducted according to the manufacturer's instructions. Briefly, hydrated tissue sections were sequentially stained with Weigert's iron hematoxylin solution, Biebrich scarlet–acid fuchsin solution, and aniline blue solution. The sections were then mounted and imaged for histological assessment.

Immunohistochemical (IHC) staining was performed to evaluate tissue regeneration and inflammation. Briefly, wound tissue sections were deparaffinized, rehydrated, and subjected to antigen retrieval by boiling in citrate buffer (100 °C). Endogenous peroxidase activity was blocked by incubating the sections with 3% hydrogen peroxide (H_2O_2) for 10–15 min, followed by washing with PBS. Sections were then incubated overnight at 4 °C with primary antibodies against collagen I (COL I; GTX26308, GeneTex, USA), TNF-α (orb371962, Biorbyt, United Kingdom), and CD31 (Clone JC/70A, Vitro.bio, Spain). After washing with PBS to remove unbound primary antibodies, the sections were incubated with either goat anti-rabbit IgG or goat anti-mouse IgG secondary antibodies (Zhongshan Biology Company, China) at 37 °C for 1 h. Immunoreactivity was visualized using 3,3′-diaminobenzidine (DAB) as the chromogenic substrate, and the sections were subsequently counterstained with hematoxylin for 2–3 min. Finally, the slides were rinsed with distilled water, dehydrated, mounted, and imaged using an optical microscope. Quantitative analysis of the positively stained area was performed using ImageJ software.

4.11. Statistical analysis

All experiments were performed at least in triplicate. Statistical significance between groups in the various results was assessed using one-way and two-way ANOVA, conducted with GraphPad Prism Software

(Version 8). A p-value of less than 0.05 ($P < 0.05$) was considered statistically significant for all tests. The significance levels were considered as follows: ****$P < 0.0001$, ***$P < 0.001$, **$P < 0.01$, and *$P < 0.05$.

Declaration of generative AI and AI-assisted technologies in the manuscript preparation process

During the preparation of this work, the authors used the ChatGPT language model to polish the English presentation. After using this service, the authors reviewed and edited the content as needed and take full responsibility for the published article.

Supporting information

Supporting information is available from nature or from the author.

Acknowledgments

Financial assistance for this research was provided by the European Union's Horizon 2020 Marie Sklodowska-Curie H2020-MSCA-ITN-ETN-2020 (no. 955335), Swedish Strategic Research Grant 'StemTherapy' (Dnr 2009-1035), and the Swedish Research Council (Dnr 2020-04025).

Conflict of Interest

The authors declare no conflict of interest.

Data Availability Statement

The data that support the findings of this study are available from the corresponding author upon reasonable request.

References

[1] A. L. Worsley, D. H. Lui, W. Ntow-Boahene, W. Song, L. Good, J. Tsui, *International Wound Journal* **2023**, *20*, 2346.

[2] S. Tavakoli, M. A. Kisiel, T. Biedermann, A. S. Klar, *Biomedicines* **2022**, *10*, 118.

[3] S. Tavakoli, A. S. Klar, *Applied Sciences* **2021**, *11*, 1493.

[4] S. Tavakoli, A. S. Klar, *Biomolecules* **2020**, *10*, 1169.

[5] "Protective and pathogenic functions of macrophage subsets | Nature Reviews Immunology," can be found under https://www.nature.com/articles/nri3073, **n.d.**

[6] X. Li, Y. Wang, B. Yuan, H. Yang, L. Qiao, *Int J Clin Exp Pathol* **2017**, *10*, 11098.

[7] S. Wang, S. Tavakoli, R. P. Parvathaneni, G. N. Nawale, O. P. Oommen, J. Hilborn, O. P. Varghese, *Biomaterials Science* **2022**, *1*, 6399.

[8] C. Yang, Y. Zhang, X. Zhang, P. Tang, T. Zheng, R. Ran, G. Li, *Carbohydrate Polymers* **2023**, *320*, 121231.

[9] S. Tavakoli, A. Kocatürkmen, O. P. Oommen, O. P. Varghese, *Advanced Materials* **n.d.**, *n/a*, 2500315.

[10] S. Wang, G. N. Nawale, O. P. Oommen, J. Hilborn, O. P. Varghese, *Polymer Chemistry* **2019**, *10*, 4322.

[11] "Design, synthesis, and in vitro antimicrobial activity of hydrazide–hydrazones of 2-substituted acetic acid - Popiołek - 2016 - Chemical Biology & Drug Design - Wiley Online Library," can be found under https://onlinelibrary.wiley.com/doi/10.1111/cbdd.12820, **n.d.**

[12] Ł. Popiołek, *Med Chem Res* **2017**, *26*, 287.

[13] F. Sellberg, F. Fredriksson, T. Engstrand, T. M. Bowden, B. Nilsson, J. Hong, F. Knutson, D. Berglund, *PLOS ONE* **2019**, *14*, e0225777.

[14] E. Martínez-Sanz, D. A. Ossipov, J. Hilborn, S. Larsson, K. B. Jonsson, O. P. Varghese, *Journal of Controlled Release* **2011**, *152*, 232.

[15] H. J. Yan, T. Casalini, G. Hulsart-Billström, S. Wang, O. P. Oommen, M. Salvalaglio, S. Larsson, J. Hilborn, O. P. Varghese, *Biomaterials* **2018**, *161*, 190.

[16] O. P. Varghese, W. Sun, J. Hilborn, D. A. Ossipov, *J. Am. Chem. Soc.* **2009**, *131*, 8781.

[17] C. Huang, L. Dong, B. Zhao, Y. Lu, S. Huang, Z. Yuan, G. Luo, Y. Xu, W. Qian, *Clin Transl Med* **2022**, *12*, e1094.

[18] E. Rahimpour, A. Haghighizadeh, M. Bagheri tabar, D. Molazemhoseini, P. Heydari, A. Banimahdidehkordi, R. Jahani, *Journal of Drug Delivery Science and Technology* **2025**, *113*, 107385.

[19] G. Chen, X. Zhu, L. Yang, T. He, B. Huang, X. Ou, L. Chen, T. Yan, S. Zhang, G. Lyu, Y. Xu, W. Dai, H. Xia, D. Yu, *Advanced Functional Materials* **n.d.**, *n/a*, e25109.

[20] P. L. Thi, Y. Lee, D. L. Tran, T. T. H. Thi, J. I. Kang, K. M. Park, K. D. Park, *Acta Biomaterialia* **2020**, *103*, 142.

[21] Y. Wang, C. Zhou, Z. Li, G. Li, Y. Zou, X. Li, P. Gu, J. Liu, L. Bai, H. Yan, J. Liang, X. Zhang, Y. Fan, Y. Sun, *Bioactive Materials* **2024**, *41*, 193.

[22] S. Mathew, T. E. Abraham, Z. A. Zakaria, *J Food Sci Technol* **2015**, *52*, 5790.

[23] S. Samanta, V. K. Rangasami, H. Sarlus, J. R. K. Samal, A. D. Evans, V. S. Parihar, O. P. Varghese, R. A. Harris, O. P. Oommen, *Acta Biomaterialia* **2022**, *142*, 36.

[24] J. S. Frenkel, *Int Wound J* **2012**, *11*, 159.

[25] M. Paidikondala, S. Wang, J. Hilborn, S. Larsson, O. P. Varghese, *ACS Appl. Bio Mater.* **2019**, *2*, 2006.

[26] M. Vetrík, M. Přádný, M. Hrubý, J. Michálek, *Polymer Degradation and Stability* **2011**, *96*, 756.

[27] M. F. Queiroz, D. A. Sabry, G. L. Sassaki, H. A. O. Rocha, L. S. Costa, *Antioxidants (Basel)* **2019**, *8*, 478.

[28] M. Shin, J. H. Galarraga, M. Y. Kwon, H. Lee, J. A. Burdick, *Acta Biomaterialia* **2019**, *95*, DOI 10.1016/j.actbio.2018.10.028.

[29] S. Tavakoli, D. Pouloutidou, O. P. Oommen, O. P. Varghese, *Materials Today Bio* **2026**, *37*, 102818.

[30] O. Krupkova, H. Greutert, N. Boos, J. Lemcke, T. Liebscher, K. Wuertz-Kozak, *Eur Spine J* **2020**, *29*, 605.

[31] K. L. Chao, L. Muthukumar, O. Herzberg, *Biochemistry* **2007**, *46*, 6911.

[32] S. Samanta, V. K. Rangasami, N. A. Murugan, V. S. Parihar, O. P. Varghese, O. P. Oommen, *Polymer Chemistry* **2021**, *12*, 2987.

[33] W. Zhang, R. Wang, Z. Sun, X. Zhu, Q. Zhao, T. Zhang, A. Cholewinski, F. (Kuo) Yang, B. Zhao, R. Pinnaratip, P. K. Forooshani, B. P. Lee, *Chem Soc Rev* **2020**, *49*, 433.

[34] K. Ukaegbu, E. Allen, K. K. H. Svoboda, *Int Wound J* **2025**, *22*, e70330.

[35] E. Mateev, M. T. Muhammed, A. Irfan, S. Sharma, M. Georgieva, A. Zlatkov, *Pharmacia* **2024**, *71*, 1.

[36] H. Boulebd, Y. Zine, I. A. Khodja, A. Mermer, A. Demir, A. Debache, *Journal of Molecular Structure* **2022**, *1249*, 131546.

[37] R. G. Frykberg, J. Banks, *Adv Wound Care (New Rochelle)* **2015**, *4*, 560.

[38] M. Kharaziha, A. Baidya, N. Annabi, M. Kharaziha, A. Baidya, N. Annabi, *Advanced Materials* **2021**, *33*, 2100176.

[39] L. Y. W. Bourguignon, P. A. Singleton, H. Zhu, B. Zhou, *J Biol Chem* **2002**, *277*, 39703.

[40] P. J. McKeown-Longo, P. J. Higgins, *Adv Wound Care (New Rochelle)* **2021**, *10*, 137.

[41] R. Zhang, W. Yang, K. Li, X. Zhang, J. Liu, L. Ai, *Arch Oral Biol* **2025**, *174*, 106237.

[42] P. Fan, Q. Dong, J. Yang, Y. Chen, H. Yang, S. Gu, W. Xu, Y. Zhou, *Carbohydrate Polymers* **2023**, *313*, 120854.

[43] Y. Shan, F. Cao, X. Zhao, J. Luo, H. Mei, L. Zhang, Y. Huang, Y. Yang, L. Yan, Y. Huang, Y. Han, B. Guo, *Biomaterials* **2025**, *315*, 122936.

[44] P. L. Thi, Y. Lee, D. L. Tran, T. T. H. Thi, J. I. Kang, K. M. Park, K. D. Park, *Acta Biomater* **2020**, *103*, 142.

[45] M. Alhajj, A. Goyal, in *StatPearls [Internet]*, StatPearls Publishing, **2022**.

[46] M. Kharaziha, S. Salehi, M. Shokri, S. M. Ahmadi Tafti, T. Scheibel, *Advanced Healthcare Materials* **n.d.**, *n/a*, e01886.

[47] D. J. Yang, S. H. Moh, D. H. Son, S. You, A. W. Kinyua, C. M. Ko, M. Song, J. Yeo, Y.-H. Choi, K. W. Kim, *Molecules* **2016**, *21*, 899.

[48] T. N. Demidova-Rice, J. T. Durham, I. M. Herman, *Adv Wound Care (New Rochelle)* **2012**, *1*, 17.

[49] Y. Zheng, K. Shariati, M. Ghovvati, S. Vo, N. Origer, T. Imahori, N. Kaneko, N. Annabi, *Biomaterials* **2023**, *301*, 122240.

[50] A. Grada, J. Mervis, V. Falanga, *Journal of Investigative Dermatology* **2018**, *138*, 2095.

Graphical abstract